

**CHARACTERIZING FLUID CONTACTS FROM
SEISMIC DATA BY JOINT INVERSION OF
ACOUSTIC VELOCITY AND IMPEDANCE**

BY

Amjad Ali

A Thesis Presented to the
DEANSHIP OF GRADUATE STUDIES

KING FAHD UNIVERSITY OF PETROLEUM & MINERALS

DHAHRAN, SAUDI ARABIA

In Partial Fulfillment of the
Requirements for the Degree of

MASTER OF SCIENCE

In

GEOPHYSICS

May, 2016

KING FAHD UNIVERSITY OF PETROLEUM & MINERALS

DHAHRAN- 31261, SAUDI ARABIA

DEANSHIP OF GRADUATE STUDIES

This thesis, written by AMJAD ALI under the direction his thesis advisor and approved by his thesis committee, has been presented and accepted by the Dean of Graduate Studies, in partial fulfillment of the requirements for the degree of **MASTER OF SCIENCE IN GEOPHYSICS**



Dr. Abdullatif A. Al-Shuhail
(Advisor)



Dr. Abdulaziz M. Al-Shaibani
Department Chairman



Prof. Michael A. Kaminski
(Member)



Dr. Salam A. Zummo
Dean of Graduate Studies



Dr. SanLinn Ismail Kaka
(Member)

28/6/16

Date

© AMJAD ALI

2016

*[This thesis is dedicated to my inspiring Brother **Dr. ASIF KHAN** and
my beloved **FAMILY** and especially to **My**
PARENTS.]*

ACKNOWLEDGMENTS

“In the name of Allah, The most Beneficent and the Most Merciful”

First of all, I would like to thank my thesis advisor Dr. Abdullatif A. Al-Shuhail from the College of Petroleum Engineering and Geosciences. The door of his office was always open and he always welcomes me whenever I encounter a problem or I had a question about my research. He always guided me in the right direction whenever I needed it.

I would like to express my sincere gratitude to the College of Petroleum Engineering and Geosciences, King Fahd University of Petroleum and Minerals, for giving me the opportunity and all the facilities to continue my education and research. I also want to thank the entire faculty member who taught me and helped me throughout my graduation.

I would like to mention special thanks to Mr. Abdul Salam and Mr. Arbab Latif, who helped me during the data generation for this thesis. I am really thankful to all Pakistani community, who encouraged me and gave me good company during my studies.

I would also like to thank my Thesis committee members, Dr. Sanlinn Ismail Kaka, and Prof. Michael A. Kaminski, for their positive contribution throughout the period of this research.]

TABLE OF CONTENTS

ACKNOWLEDGMENTS.....	V
TABLE OF CONTENTS.....	VI
LIST OF TABLES.....	IX
LIST OF FIGURES.....	X
LIST OF ABBREVIATIONS.....	XII
ABSTRACT.....	XIII
ملخص الرسالة.....	XV
1 CHAPTER 1 INTRODUCTION.....	1
1.1 Background.....	1
1.2 Objectives.....	4
1.3 Literature Review.....	4
1.3.1 Well Logs data to identify pore fluid.....	4
1.3.2 Seismic and well logs derived attributes.....	8
1.3.3 AVO analysis for fluid characterization.....	16
1.3.4 Gassmann's equation to mark OWC/GWC.....	16
2 CHAPTER 2 METHODOLOGY.....	15
2.1 Geological Model.....	15
2.2 Fluid Properties.....	16
2.2.1 Gas properties.....	16
2.2.2 Live oil properties.....	19

2.2.3	Brine water properties	21
2.3	Matrix properties of reservoir.....	23
2.4	Velocity and density model.....	23
2.5	Gassmann's equation for fluid substitution	24
2.6	Fluid identification	27
3	CHAPTER 3 SEISMIC DATA GENERATION	30
3.1	Synthetic seismogram	30
3.1.1	Case-1.....	30
3.1.2	Case-2.....	33
4	CHAPTER 4 RESULT AND DISCUSSION	35
4.1	Case-1	30
4.1.1	AI inversion	35
4.1.2	Compressional modulus (M).....	37
4.1.3	Saturated rock density (ρ_s).....	39
4.1.4	Fluid density (ρ_f)	41
4.1.5	Fluid velocity (V_f).....	43
4.2	Case-2	45
4.2.1	AI inversion	45
4.2.2	Compressional modulus (M).....	47
4.2.3	Saturated rock density (ρ_s).....	49
4.2.4	Fluid density (ρ_f)	51
4.2.5	Fluid velocity (V_f).....	53
4.3	Case-3	55
4.4	Matrix properties of reservoir.....	57

4.5	Velocity and density model	57
4.6	10% Porosity.....	58
4.6.1	Fluid density (ρ_f)	58
4.6.2	Fluid velocity (V_f).....	60
4.7	20% Porosity.....	62
4.7.1	Fluid density (ρ_f)	62
4.7.2	Fluid velocity (V_f).....	64
4.8	30% Porosity.....	66
4.8.1	Fluid density (ρ_f)	66
4.8.2	Fluid velocity (V_f).....	68
5	CHAPTER 5 CONCLUSIONS AND RECOMMENDATIONS	70
5.1	Conclusions.....	70
5.2	Recommendations.....	73
	REFERENCES.....	74
	VITAE.....	78

LIST OF TABLES

Table 2-1 Assumptions	16
Table 2-2 Computed Properties of gas.....	19
Table 2-3 Computed Properties of live-oil	21
Table 2-4 Computed Properties of brine water.....	23
Table 2-5 Velocity and density model	24
Table 2-6 Computed parameters of reservoir fully saturated with gas.....	26
Table 2-7 Computed parameters of reservoir fully saturated with live oil.....	26
Table 2-8 Computed parameters of reservoir fully saturated with brine water	27
Table 4-1 Assumed parameters of Arab formation.....	56
Table 4-2 Live oil properties for the Arab formation	56
Table 4-3 Brine properties for the Arab formation.....	56
Table 4-4 Velocity and density model for Arab formation.....	57
Table 5-1 Changes in percent in AI, M and ρ_f	70
Table 5-2 Changes in percent in fluid density and fluid velocity	71
Table 5-3 Percent error analysis in the Arab formation.....	72

LIST OF FIGURES

Figure 1.1: Effects of electrodes spacing on apparent resistivity	5
Figure 1.2: Velocity and density variation with depth for the clean water-filled sand, Gevers, and S.W. Watson (1978).....	6
Figure 1.3: Cross plot between Density (RHOB) and Neutron log (PHIN), Rirbal Singh et al., (1998)	7
Figure 1.4: Cross-plot between Vp/Vs ratio vs shear wave travel time in a water-bearing sand formation the line can be used for Hydrocarbon indicator, D. Michael Williams (1990)	9
Figure 1.5: Workflow of simultaneous AVO inversion (Kim et al., 2004).....	11
Figure 1.6: Attenuation coefficient α as Function of frequency for type-II waves, Dutta and Ode (1983)	13
Figure 2.1: Geological model.....	15
Figure 3.1: Reflection coefficient plot of case-1	31
Figure 3.2: Minimum phase wavelet plot.....	32
Figure 3.3: Trace of case-1	32
Figure 3.4: Reflection coefficient plot of case-2	33
Figure 3.5: Trace of case-2.....	34
Figure 4.1: Acoustic impedance plot of case-1	36
Figure 4.2: Compressional modulus plot of case-1	38
Figure 4.3: Saturated rock density plot of case-1	40
Figure 4.4: Fluid density plot of case-1.....	42
Figure 4.5: Fluid velocity plot of case-1	44

Figure 4.6: Acoustic impedance plot of case-2	46
Figure 4.7: Compressional modulus plot of case-2	48
Figure 4.8: Saturated rock density plot of case-2	50
Figure 4.9: Fluid density plot of case-2.....	52
Figure 4.10: Fluid velocity plot of case-2	54
Figure 4.11: Fluid density plot with 10% porosity of Arab formation.....	59
Figure 4.12: Fluid velocity plot with 10% porosity of Arab formation	61
Figure 4.13: Fluid density plot with 20% porosity of Arab formation	63
Figure 4.14: Fluid velocity plot with 20% porosity of Arab formation	65
Figure 4.15: Fluid density plot with 30% porosity of Arab formation.....	67
Figure 4.16: Fluid velocity plot with 30% porosity of Arab formation	69

LIST OF ABBREVIATIONS

OWC	Oil-water contact	API	American Petroleum Institute
GWC	Gas-water contact	PPM	Part per Million
GOC	Gas-oil contact	AI	Acoustic Impedance
M	Compressional Modulus	Vs	S-wave velocity
Vp	P-wave velocity	Rhos	Saturated rock density
T	Temperature	Rhof	Fluid density
P	Pressure	Kf	Fluid modulus

ABSTRACT

Full Name : [Amjad Ali]

Thesis Title : [Characterizing fluid contacts from seismic data by joint inversion of acoustic velocity and impedance]

Major Field : [Geophysics]

Date of Degree : [May, 2016]

In the early days, the seismic exploration technique was mainly used for gathering information about subsurface rock structures and fluids by analyzing the travel time, reflection amplitude, and phase variations. However, nowadays, many additional seismic attributes have been introduced by the seismic interpreters, which aid in the visualization of subsurface geological structures, facies, and lithologies. This research characterizes the pore fluids at the reservoir level from seismic data. Gassmann's equation is well known for fluid substitution with some assumptions and it is used for fluid substitution in this research. This research aims to identify the pore fluids in the reservoir using seismic data without requiring well log data. This is tested using a three-layer geological anticline model in which the third layer is a reservoir that is fully saturated with water, except its top part that is fully saturated with petroleum. Fluid identification is done in terms of their density, velocity changes, bulk modulus of the fluid, and acoustic impedance (AI). P-wave velocity and AI are measured from surface seismic data from which the saturated rock density and compressional modulus (M) are calculated. Finally, saturated rock density and compressional modulus are inverted for fluid velocity and density, respectively, to identify the pore fluid

In both cases, AI, compressional bulk modulus, and saturated rock density inversion gave good evidence of the presence of two different pore fluids in the reservoir. Results of fluid density and fluid velocity give good evidence and information about the pore fluids and are a helpful tool in identifying the pore fluids in the reservoir. The percent error between the inverted fluid density/velocity and the computed fluid density/velocity for gas, live oil, and brine is almost 0% for cases 1 and 2. We also apply the above approach on synthetic seismic traces representing the Arab formation of Saudi Arabia within a range of porosities. The inversion of these cases also results in similarly small error between the inverted and true fluid properties.

ملخص الرسالة

الاسم الكامل: أمجد علي

عنوان الرسالة: تمييز تماس الموانع من البيانات السايزمية بطريقة العكس المشترك للسرعة و المقاومة الصوتية

التخصص: جيوفيزياء

تاريخ الدرجة العلمية: مايو 2016

في الماضي كانت تقنيات الاستكشاف السايزمي (الزلزالي) تستخدم بشكل أساسي لجمع المعلومات عن التراكيب الصخرية و الموانع التحت سطحية عن طريق تحليل الأوقات المتطلبة لمسيرة الموجات السايزمية, و عن طريق ساعات و أطوار الموجات المنعكسة. أما الآن فقد ظهر استخدام العديد من الصفات السايزمية المميزة الجديدة من قبل المفسرين السايزميين, و التي تساعد على تصور التراكيب الجيولوجية التحت سطحية, و السحنات, و الخصائص الصخرية. في هذا البحث سيتم تمييز الموانع المسامية على مستوى الخزانات من البيانات السايزمية. معادلة غاسمان هي معادلة معروفة لاستبدال الموانع مع بعض الافتراضات و ستستخدم لاستبدال الموانع في هذا البحث. هذا البحث يهدف إلى تحديد الموانع المسامية في الخزانات باستخدام البيانات السايزمية بدون الحاجة إلى بيانات سجلات الآبار. سيتم اختبار النتائج باستخدام نموذج طية محدبة من ثلاث طبقات جيولوجية. في هذا النموذج ستكون الطبقة الثالثة هي خزان مشبع كلياً بالماء ما عدا الجزء العلوي منه فهو مشبع كلياً بالنفط. تحديد الموانع يتم عن طريق الكثافة, تغيير السرعات السايزمية, معامل الحجم للمائع, و المقاومة الصوتية. سرعات موجات "بي" و المقاومة الصوتية يتم قياسها من البيانات السايزمية السطحية, و التي يتم من خلالها حساب كثافة الصخور المشبعة و المعامل الانضغاطي "إم". أخيراً, يتم القيام بطريقة العكس لكثافة الصخور المشبعة و المعامل الانضغاطي "إم" إلى السرعة السايزمية في الموانع و إلى الكثافة على التوالي لمعرفة نوع المائع المسامي.

في كلا الحالتين فقد تم الحصول من طريقة العكس على نتائج للمقاومة الصوتية و معامل الحجم الانضغاطي و كثافة الصخور المشبعة تدل على وجود نوعين مختلفين من الموانع المسامية في الخزان. نتائج كثافة الموانع و السرعة السايزمية في الموانع تعطي معلومات و دلالات واضحة عن المائع المسامي و هي أدوات مفيدة لتحديد نوع المائع المسامي في الخزانات. نسبة الخطأ بين الكثافة و السرعة التي تم الحصول عليها بطريقة العكس و بين

تلك التي تم حسابها للنفط و الغاز و المحاليل الملحية تقارب الصفر بالمئة في الحالة الأولى و الثانية. كما تم تطبيق الطريقة السابقة على بيانات سايزمية اصطناعية تمثل مكون عرب ذات مدى محدد من المسامية و قد جاءت النتائج أيضا بنسبة خطأ ضئيلة جدا.

CHAPTER 1

INTRODUCTION

1.1 Background

In a typical hydrocarbon reservoir, the gas is commonly present at the top followed by oil that sits on top of the water. This sequence is mainly due to buoyancy produced by the difference in densities of fluids. There is often a sharp contact among the gas-, oil-, and water-saturated zones of the reservoir, which are referred to as the oil-water contact (OWC), gas-oil contact (GOC), or gas-water contact (GWC). The identification of fluids at the reservoir and the marking of this OWC/GOC/GWC are essential for the volumetric calculation of oil reserves of an oil reservoir (Chombarti, 1960). For example, for the computation of water saturation (S_w), one needs to define OWC in a wellbore.

The subsurface can be modeled to a number of layers, in which the layer thickness and lithology can be homogeneous or heterogeneous. Each layer has its own acoustic velocity and density, which mainly depends on the lithology, porosity, and pore fluid. Acoustic impedance (AI), which is the product of density and acoustic velocity, also depends on the above factors.

During hydrocarbon exploration, explorers look for a subsurface structure with high porosity because the hydrocarbon tends to accumulate in these structures. Usually, places

where hydrocarbon accumulates have relatively low acoustic velocity, density, and AI. These are good indicators of the presence of hydrocarbon.

Gassmann's equation (1951) has been widely used in the field of geophysics. It has been mainly used to observe the effect of fluid substitution on the seismic properties, such as velocity changes. The main purpose of Gassmann's equation is to compute the fluid bulk modulus. Rocks are commonly composed of rock-forming minerals that have frame/skeleton, the solid matrix, and pores, pore fluids that can be gas, oil, or water. Gassmann's equation can be defined as:

$$K_s = K_d + \frac{\left(1 - \frac{K_d}{K_m}\right)^2}{\frac{\emptyset}{K_f} + \frac{1-\emptyset}{K_m} - \frac{K_d}{K_m^2}} \quad (1.1)$$

where K_s is saturated rock bulk modulus, K_d is dry rock bulk modulus, K_m bulk modulus of the matrix, K_f is fluid bulk modulus and \emptyset is porosity.

Gassmann's equation is based on the following assumptions:

1. Porous rock is isotropic, elastic and homogeneous at the macroscopic scale.
2. The pore spaces in the rock are well interconnected and there is pressure equilibrium.
3. Pore spaces are filled with a frictionless fluid such as gas, oil, water, or a mixture.
4. It is a closed system, with no fluid movement across the boundaries.
5. There is no chemical interaction between fluid and rock.

This study investigates the effects of pore fluids on seismic data to characterize the pore fluid. The characterization of fluids at the reservoir level using seismic data in the

absence of well log data will be a very helpful tool in the development of a new oil and gas field. It will help also in the estimation of reserves before drilling new wells and will increase the chances of success.

Different techniques have been developed in the past to identify and mark the OWC/GOC/GWC, including mud logs, core analysis, resistivity log, and neutron log.

a) Mud logs

Mud logs are records of drilling mud contents including, gas/oil composition, quantities, description, and analysis. This provides the information about the lithology and fluid contents of different formations. To mark the OWC/GOC/GWC, depth versus mud log analysis data is plotted, which indicate the reservoir's top and oil/gas/water contents.

b) Core analysis

Core analysis provides the direct indication of oil, gas or water contents due to the presence of stains of high concentration of oil/gas.

c) Resistivity

Resistivity is another method to mark the OWC/GOC/GWC. The whole resistivity logging is based on Archie's equation, which relates the resistivity of the formation to the resistivity of fluid in the formation. The resistivity of formation depends on the porosity, S_w , and matrix resistivity. By observing the logging curve and using Archie's equation, one can identify fluids and calculate the S_w to mark the OWC//GOC/GWC.

1.2 Objectives

The main objective of this study is to characterize the pore fluid in a reservoir by the joint inversion of the acoustic (P-wave) velocity and (P-wave) impedance calculated from surface seismic data with no input from a well log or other direct methods.

Other objectives can be summarized as follows:

- Generation of synthetic seismic data
- Inversion of AI
- Computation of density and compressional modulus (M)
- Inverting the AI, acoustic velocity, density, and compressional modulus for the pore fluid density and velocity.

1.3 Literature review

1.3.1 Well log data to identify pore fluid

Many developments have taken place in the field of well logging in the last 25 years. Archie (1960) was the first person who defined the term “petrophysics”, and now it has become the science of borehole geophysics (Snyder and Fleming, 1985).

Doll et al. (1947) presented a method to compute true resistivity from apparent resistivity, which is recorded in the borehole, and the relationship of electrode spacing and mud resistivity. True resistivity has an important role in identifying fluid saturation in different zones of the reservoir marking the OWC/GWC and for the estimation of reserves. He discussed the effect of electrode spacing on apparent resistivity, as shown in Figure 1.1.

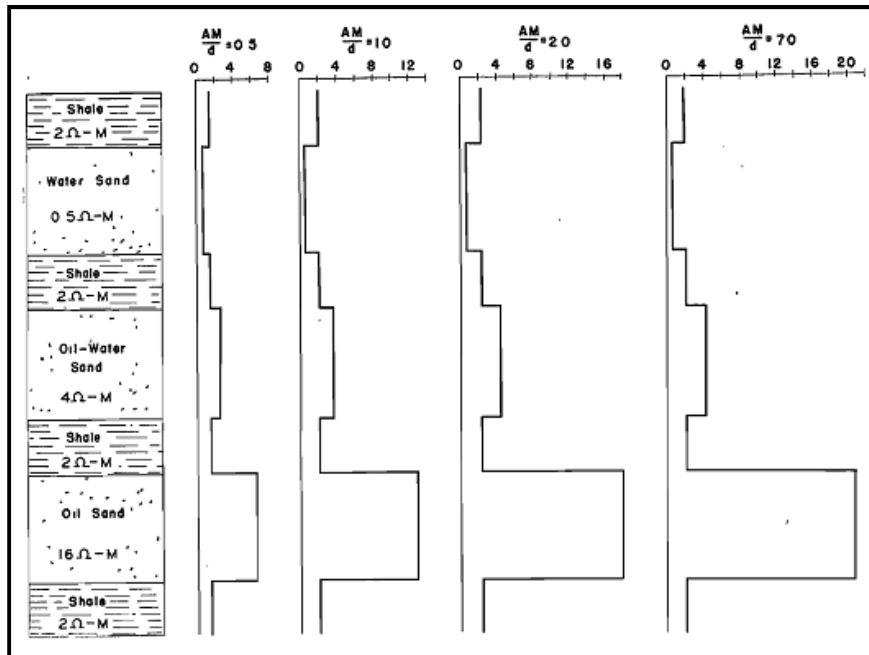


Figure 1.1: Effects of electrodes spacing on apparent resistivity

Wylie (1952) worked on the idea of combining of neutron and resistivity logs for computation of porosity, oil saturation zones, and estimation of connate water. To correlate the neutron and resistivity logs for direct plotting, he introduced the idea of formation factor unity for the neutron log deflection.

Chombarti (1960) presented a summary of different logging techniques and their interpretation that is used for the carbonate reservoir. He provided a detailed plan for carbonate reservoir study. Based on that, all the cutting and cores should be properly handled and should precisely mention their rock type and depth. Furthermore, one should choose those logging techniques, which provide the maximum number of information about the reservoir and can be used for further statistical models. Finally, one should do the laboratory test of core data and correlate it with logging data to define the reservoir in more detail. Furthermore, for S_w , one should use capillary pressure test along with logging data.

Gevers and Watson (1978) proposed three-stage processes for quantitative interpretation of the formation using the well log data. According to this process, it initially generates acoustic log data for every 0.5 ft, then calibrates the acoustic log data with AI, and at the third and final stage calculates and collects the rock physics parameters and also generates a graph for the variation of density and velocity with depth to delineate the hydrocarbon zones, as shown in Figure 1.2.

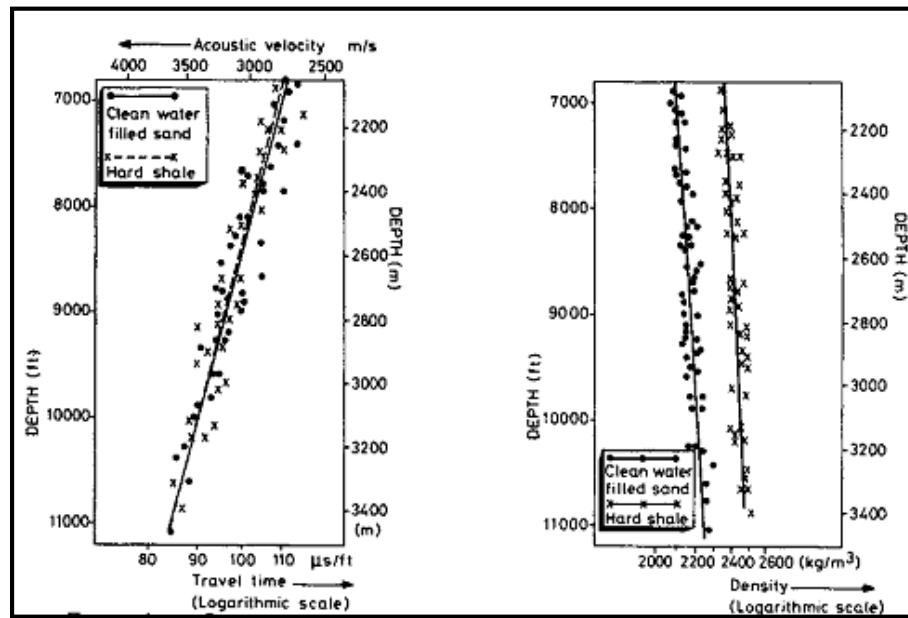


Figure 1.2: Velocity and density variation with depth for the clean water-filled sand (Gevers and Watson, 1978)

Usually, OWC/GWC are identified using resistivity log data; however, due to some borehole problems or high inclination, it is difficult to identify OWC/GWC for perforation purposes. In such case, variable density log (VDL) and cement bonding log (CBL) are useful tools. The main purpose of the VDL and CBL is to check the bonding quality between case-cement and cement-formation. VDL is the continuous recording of P-wave transit time among the casing, cementing, and formation. The P-wave attenuation is inversely proportional to formation density. In a reservoir formation, which has an oil

and water layer with the same lithology and porosity range, the P-wave transit time in oil will be higher than water due to its low density (Pande, 1983).

In a case study in India, which has a complex lithology, it was difficult for the petrophysicist to identify GOC and OWC. To solve this problem, they developed a methodology that included the study of well logs, the cross-plot of different lithologies, F-overlay, and sonic log versus neutron log overlay. To identify the major lithology and type of hydrocarbon in specific zones, a cross-plot between densities versus neutron was drawn, as shown in Figure 1.3. Then, the formation factor (F overlay) was computed using the resistivity log and sonic neutron log, and F-overlay was done on a logarithmic scale. Based on the above methodology, GOC and OWC were established (Singh et al., 1998).

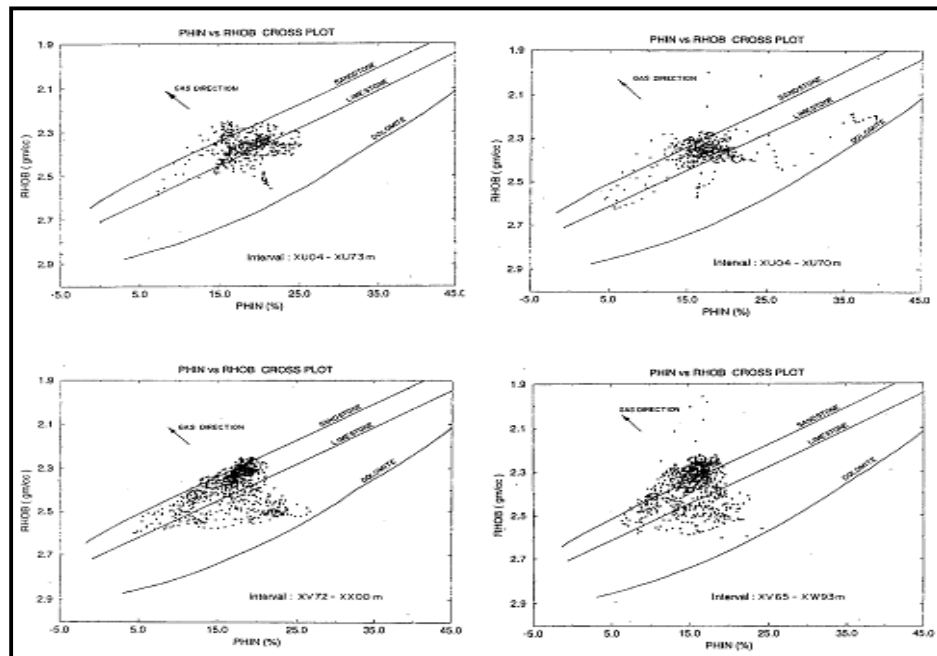


Figure 1.3: Cross plot between density (RHOB) and Neutron log (PHIN) (Singh et.al., 1998)

Well log data were collected and then petrophysical interpretation was performed, which included the determination of porous zones, volume of shale, water, and hydrocarbon-bearing zones and oil water contact. S_w was found using the true resistivity of water in the uninvaded zone. Finally, hydrocarbon saturation was computed. After the interpretation of the well log, it has been found that there are 10 hydrocarbon zones whose thickness varies from 11 to 90 ft and the oil water contact is marked at 2229 ft due to the change in resistivity log (Jarot and Ariffin, 2006).

1.3.2 Seismic and well log derived attributes

In Campose Basin, Brazil, anomalous amplitudes were found just below the target horizon. Initially, it was assumed that this is due to lithological changes in the vertical direction, but later it was found that the position of these anomalous amplitudes was present at the depth of OWC, which was confirmed by well log data. Later, it was concluded that it was caused by a change in AI due to fluid change. To confirm this hypothesis, they used the Biot-Geertsma model for frequency (Domenico, 1974; Catto, 1980). Finally, the measured values were incorporated to match the velocities for both water- and oil-saturated zones. Then, the seismic data were reinforced with the modeling data; as a result, the target reflector disappeared and a prominent reflector appeared, which coincided with the OWC of the nearest well (AndrkLuiz et al., 1985).

Fluid saturation strongly affects the propagation of P-waves in a formation but has no effect on S-wave propagation, as the fluid does not have the shear component. By considering these facts, Williams (1990) developed an algorithm for hydrocarbon identification, which he named acoustic log hydrocarbon indicator (ALHI). Basically,

this algorithm is applied to clastic rocks, where the aim is to differentiate the water-bearing zone from the hydrocarbon-bearing zone. This algorithm is more effective in younger and unconsolidated formations and has been successfully applied in Cretaceous to Plio-Pleistocene hydrocarbon-bearing formations, as shown Figure 1.4. The integration of seismic and petrophysical data is very important to map and to detect both hydrocarbon-bearing zones.

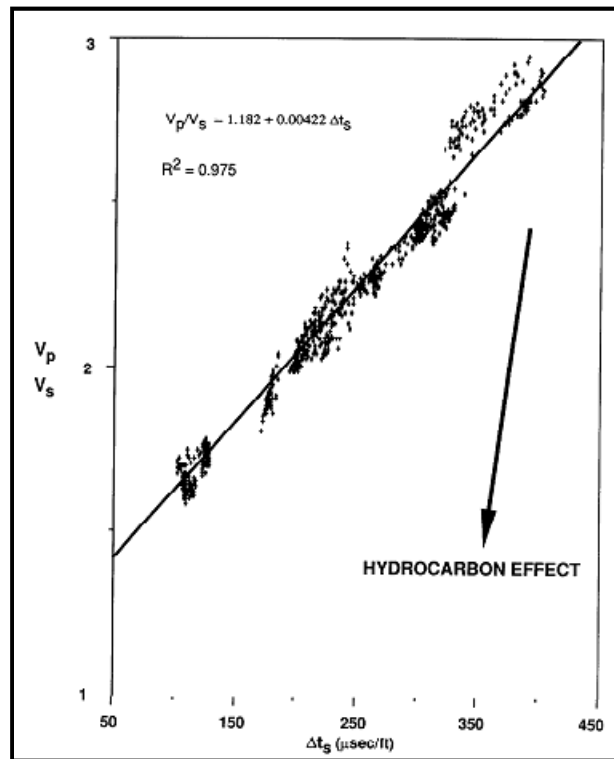


Figure 1.4: Cross-plot between V_p/V_s ratio vs. shear wave travel time in a water-bearing sand formation. The line can be used as a hydrocarbon indicator (Williams, 1990)

Theodoros Klimentos (1995) used three well data to gauge the P- and S-wave attenuation from sonic data using the spectral peak method. Due to P- and S-wave attenuation, a gas condensate in clean sandstone was marked with the S_w ranging from 25% to 30%, whereas, on the contrary, the neutron and density log did not show any prominent crossover for the indication of gas condensate zone.

In the Puerto Colon Field, Colombia, it was suggested that there are three different reservoirs, but later on different production data and testing did not support this assumption. To solve this problem for the better understanding of the reservoir, a geostatistical model (Peña et al., 1999) was applied. A 3D facies model has generated a model that included the structure of the reservoir formation, porosity, and permeability. Initially, free water level (FWL) was determined using petrophysical data, RFT, DST, and special core analysis. Then, OWC was determined using petrophysical analysis. Finally, the true and actual resistivity of saline water was found by the quality control of the data, which confirmed that the OWC is tilted (Carlos, 2000).

1.3.3 AVO analysis for fluid characterization

Chiburis (1984, 1987b) worked on the idea of AVO application in Saudi Arabia for pore fluid characterization in the reservoir and detecting OWC. For this study, six different areas have been investigated in which three of them are offshore and three of them are onshore in the eastern province of Saudi Arabia. One of them is marine area 2, which has an oil carbonate reservoir at a depth of 2400 m. There are two structures present in this area and both are oil reservoir followed by brine. AVO inversion for three lines on both structures gave positive AVO and was able to delineate the OWC for both structures.

Kim et al. (2004) worked on the idea of simultaneous AVO inversion to estimate the subsurface rock properties such as AI, Poisson's ratio, shear impedance, and density. In AVO, the angle of incident is an important parameter and it is obtained from seismic processing velocities. The workflow is shown in Figure 1.5.

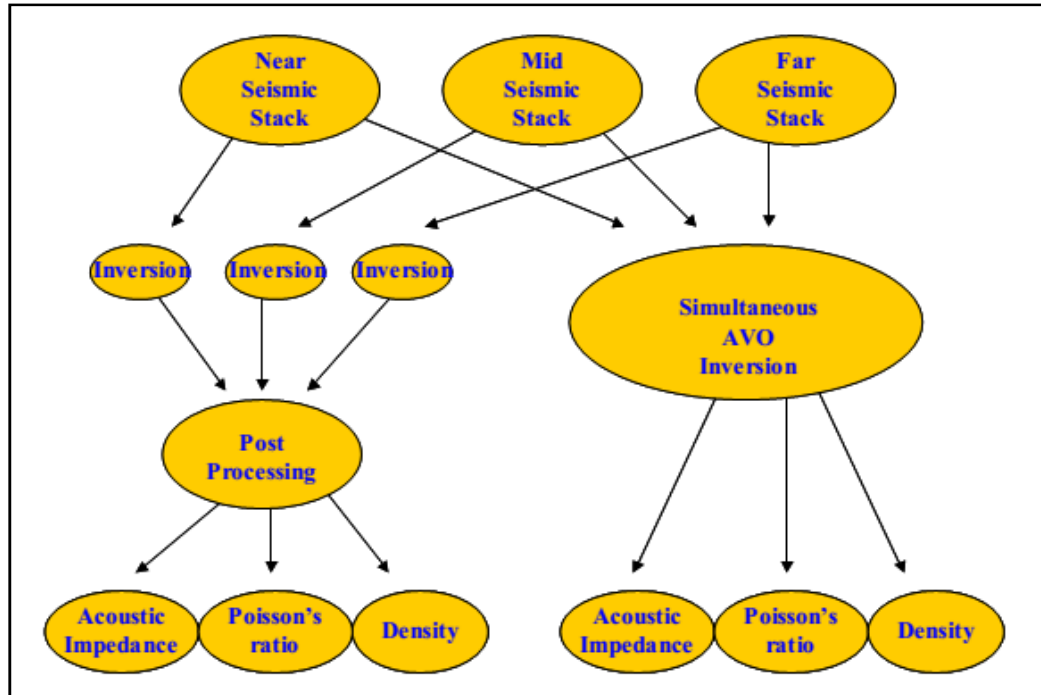


Figure 1.5: Workflow of simultaneous AVO inversion (Kim et al., 2004)

Andrew et al. (2004) did the AVO analysis for Bin Nevis Reservoir, Canada, to find the API variation in the reservoir and differentiate the pore fluid in the reservoir. Using the fluid factor analysis gave the picture of the reservoir and showed the boundary between the oil and water, which is assumed as the OWC. The cross-plot of P- and S-wave reflectivity series separated the two different pore fluids in the reservoir.

Chi and Han (2007) studied the reservoir properties using the AVO attributes. They linked the rock physics model with AVO attributes to understand the reservoir properties. Through the AVO attributes, the clay content, S_w , and porosity are estimated. They used the shaley-sand model, in which they computed the elastic properties of the model. They applied the AVO inversion through which they got the P- and S-wave velocities, which is later linked with the rock physics model for the detailed picture of the reservoir.

Kato and Stewart (2012) did the AVO inversion for time-lapse elastic reservoir properties. In time-lapse data, they did the AVO inversion for both baseline and monitor survey data to obtain simultaneously elastic properties such as P-wave, S-wave, velocities, and density along with the uncertainties. During the inversion, they used the individual wavelet for both data sets. The final results reasonably agreed with well log data.

Li and Zhang (2015) did the direct estimation of petrophysical properties from AVO inversion. They interlinked the rock physics model and AVO inversion attributes to get information about reservoir properties. Initially, they did the linear regression analysis of the well data to obtain the rock physics model and then they obtained the reflection coefficient (RC) equation for the incorporation of the rock physics model with Aki's RC. Finally, the AVO inversion was done for reservoir parameters.

1.3.4 Gassmann's equation to mark OWC/GWC

Using the boundary value problem, Dutta and Ode (1983) calculated the loss of amplitude and RC. To show the effect of pore fluid on seismic reflection, they used P-wave reflection and transmission at an oblique angle between two porous rocks where the upper part contained gas and the lower part was filled with brine. According to this model, most of the attenuation is due to mode conversion to type II, as shown in Figure 1.9. It was observed that, for the porous unconsolidated sandstone, the loss of energy is almost 2.5% for the compressional wave when the frequency was 100 Hz and the angle of an incident was 30°. It was found that the loss of energy increases with $f^{1/2}$. On the contrary, the amplitude of RC decreases at GWC with the increase of frequency at all

incident angles. In this model, the decrease is approximately about 1.5% to 3%. It has been found that the V_p for brine is 7234 ft/s as a pore fluid and 4920 ft/s for gas V_p and V_s is 3044 ft/s, whereas the porosity is 0.3 and the permeability is 1 Darcy.

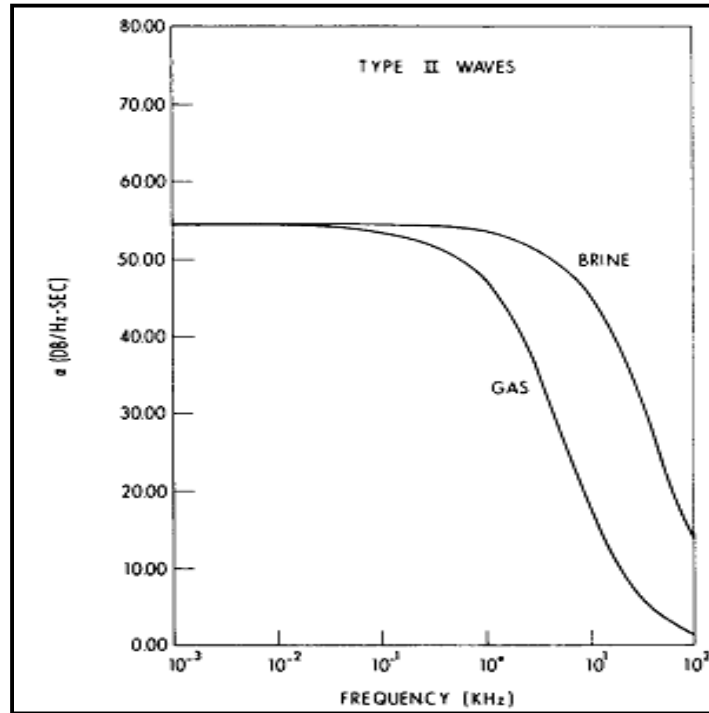


Figure 1.6: Attenuation coefficient α as Function of frequency for type-II waves, (Dutta and Ode, 1983)

Ratnamoorthy and Murphy (1998) worked to identify the pore fluid in limestone using rock mechanics. First of all, they collected the shear and compressional wave velocity along with the other standard well logs. Bulk and shear moduli of the formation were determined. Then porosity is further divided into two parts, intergranular and spherical, which help to compute the appropriate K_b/G ratio. Then, the bulk modulus of fluid was found using Gassmann's equation. Usually, the bulk modulus of water is 3 GPa, it is almost zero for gas, and it ranges from 0 to 3 GPa for oil depending on the density and gas/oil ratio. The compressional velocity was then modeled, which had been measured in

the borehole for the forward modeling of the corresponding fluid. Finally, by comparing the modeled velocity with measured velocity, the pore fluid was identified.

In this thesis, I used the density and Gassmann's equations to invert the pore fluid properties from P-wave velocity and AI estimated from surface seismic data. I applied the method on synthetic seismic traces generated for a typical anticline model and the Arab limestone reservoir of Saudi Arabia.

This thesis is organized in five chapters. Chapter 1 gives an introduction with a relevant literature. Chapter 2 gives the details of the methods and procedures used in my proposed algorithm. Chapter 3 discusses the models used to generate synthetic data and how synthetic data were generated. Chapter 4 outlines the main results of this study. Chapter 5 presents the salient conclusions of this study and recommendations for further work.

CHAPTER 2

METHODOLOGY

2.1 Geological model

The geological model comprised three layers, as shown in Figure 2.1. The surface to the top of the second layer is assumed as one layer, the second layer is shale that acts as a cap rock, and the third layer is pure sandstone that is the reservoir in this model. The lateral extension of the model is 4000 m and the vertical depth is 3000 m. The maximum curvature of the geological model is 400 m at the reservoir level, where the maximum thickness of oil column in the reservoir is 200 m and the remaining part is fully water saturated.

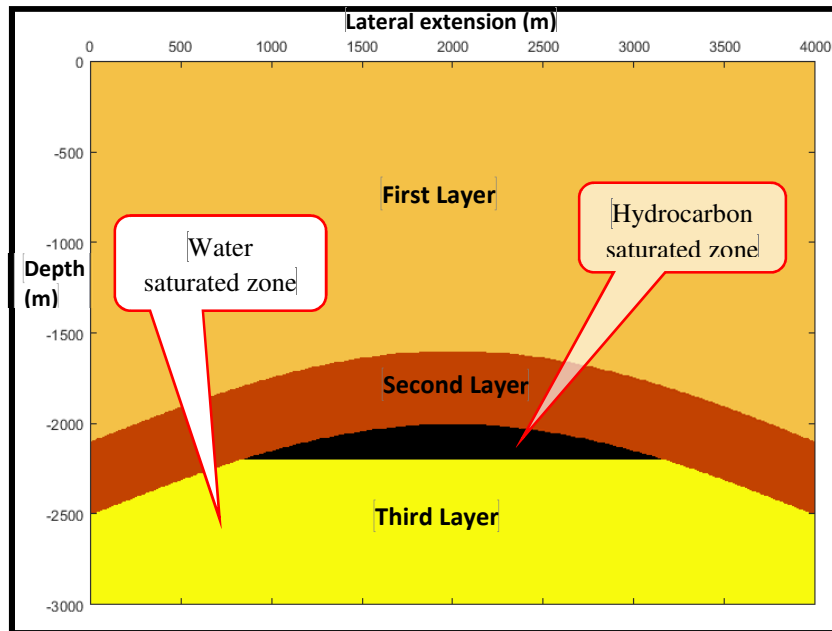


Figure 2.1: Geological model

There are few assumptions made about the model, which are given in Table 2.1.

Table 2-1: Assumptions

Porosity	Reservoir porosity	20%
T (°C)	Temperature at reservoir level	150
Depth (m)	Reservoir depth at crest	1600

2.2 Fluid properties

In this model, Gassmann’s equation is used for fluid substitution to observe the effects on seismic properties due to pore fluid. Three different fluids (gas, live oil, and water) are used to compute the seismic and elastic properties of the reservoir fluid. The properties of these three fluids are computed and described below.

2.2.1 Gas properties

Generally, gas is characterized by the ratio of gas density to air density. Here, I used methane gravity for fluid substitution and the gravity of gas is 0.56. The density of gas is calculated using following empirical equations.

First, I had to determine the absolute temperature using the following Kelvin equation:

$$T_a = T + 273 \tag{2.1}$$

T_a is the absolute temperature (Kelvin) and T is 150°C temperature at the reservoir level.

Pressure in MPa at the reservoir level is computed using pressure water gradient equation:

$$P = ((D * 0.433) + 14.7) * 0.006894757293178 * 3.28 \tag{2.2}$$

where P is the pressure (psi) and D is the depth (m). Next, I computed the pseudo-pressure and pseudo-temperature following the Batzle and Wang (1992) equation equations:

$$P_r = \frac{P}{4.892 - 0.4048 * G} \quad (2.3)$$

$$T_r = \frac{T_a}{94.72 + 170.75 * G} \quad (2.4)$$

T_a and P are the pressure and temperature at the reservoir level, respectively; and G is the gas/oil ratio, which is in this case 0.56.

Finally, the density of the gas is computed using the Batzle and Wang (1992) equation as

$$\rho_g = \frac{28.8 * G * P}{Z * R * T_a} \quad (2.5)$$

where ρ_g is the density of gas in g/cm^3 , G is the gas/oil ratio, P is the pressure (MPa), T_a is the absolute temperature, and R is the gas constant (which is 8.31441 J/g/mole deg). Z is computed Batzle and Wang (1992) equation as:

$$Z = aP_r + b + cd \quad (2.6)$$

Where,

$$a = 0.03 + 0.00527(3.7 - T_r)^3 \quad (2.7)$$

$$b = 0.642T_r - 0.007T_r^4 - 0.52 \quad (2.8)$$

$$c = 0.109(3.85 - T_r)^2 \quad (2.9)$$

$$d = EXP \left\{ - \left[0.45 + 8 * \left(0.56 - \frac{1}{T_r} \right)^2 \right] \frac{P_r^2}{T_r} \right\} \quad (2.10)$$

The bulk modulus of the gas is computed using the following equation (Batzle and Wang, 1992):

$$K_g = \frac{P\gamma}{1 - \frac{P_r}{Z}f} \quad (2.11)$$

where

$$\gamma = 0.85 + \frac{5.6}{P_r+2} + \frac{27.1}{(P_r+3.5)^2} - 8.7e^{-0.65(P_r+1)} \quad (2.12)$$

$$f = cdm + a \quad (2.13)$$

$$m = 1.2 \left\{ - \left[0.45 + 8 * \left(0.56 - \frac{1}{T_r} \right)^2 \right] \frac{P_r^{0.2}}{T_r} \right\} \quad (2.14)$$

The results of these equations are given in Table 2.2.

Table-2.2: Computed properties of gas

P (MPa)	21.1600
Ta (K)	423.15
Tr (K)	2.2231
Pr (MPa)	4.5356
Z	0.9858
ρ_g (g/cm ³)	0.0946
m	-0.3996
v	10.378
f	0.01202
K _g (Pascal)	21960

2.2.2 Live oil properties

The density of the live oil is computed using the following equation (Batzle and Wang, 1992):

$$R_g = 0.02123 G \left[P \text{ EXP} \left(\frac{4.072}{\rho_o} - 0.00377T \right) \right]^{1.205} \quad (2.15)$$

R_g is the volume ratio of liberated gas to remaining gas, G is the gas gravity that for this model is assumed that methane is dissolved in oil with gas gravity equal to 0.56, T is the temperature, and P is computed for live oil at 2150 m. To get the true density, first a pseudo-density ρ' should be computed using the following equation (Batzle and Wang, 1992):

$$\rho' = \frac{\rho_o}{B_o} (1 + 0.001 R_g)^{-1} \quad (2.16)$$

ρ_o is computed as:

$$\rho_o = \frac{141.5}{\text{API} + 131.5} \quad (2.17)$$

where API of the live oil is assumed as 42.

B_o is the oil formation volume factor that is calculated using the following equation (Batzle and Wang, 1992):

$$B_o = 0.972 + 0.00038 \left[2.4 R_g \left(\frac{G}{\rho_o} \right)^{1/2} + T + 17.8 \right]^{1.175} \quad (2.18)$$

The density of the oil with dissolved gas is given as (Batzle and Wang, 1992):

$$\rho_g = (\rho_o + 0.0012GR_g) / B_o \quad (2.19)$$

Now this density should be corrected for pressure to find actual density ρ_p as (Batzle and Wang, 1992):

$$\rho_p = \rho_g + (0.00277P - 1.71 * 10^{-7}P^3)(\rho_g - 1.15)^2 + 3.49 * 10^{-4}P \quad (2.20)$$

The velocity of the live oil is computed using the following equation (Batzle and Wang, 1992):

$$V_p = 2096 \left(\frac{\rho'}{2.6 - \rho'} \right)^{1/2} - 3.7T + 4.64P + 0.0115 \left[4.12(1.08\rho'^{-1} - 1)^{1/2} - 1 \right] TP \quad (2.21)$$

The bulk modulus of live oil is computed as:

$$K_o = (\rho * V_p) 10^{-6} \quad (2.22)$$

Table-2.3 presents the computed values for all parameters of live oil using the above equations for density, velocity, and bulk moduli.

Table-2.3: Computed properties of live oil

G	0.56
P (GPa)	0.0212
R _g	0.0237
B _o (bbl/STB)	1.1283
ρ' (g/cm ³)	0.7228
ρ _g (g/cm ³)	0.7228
ρ _p (g/cm ³)	0.7229
V _p (m/sec)	745.7754
K _o (Pascal)	402040000

2.2.3 Brine water properties

To find the density of brine water, the salinity of water should be known, which is assumed as 84,000 ppm, and the density of brine of water is computed as (Batzle and Wang, 1992):

$$\rho_b = \rho_w + S\{0.668 + 0.44S + 10^{-6}[300P - 2400P * S + (80 + 3T - 3300S - 13P + 47P * S)]\} \quad (2.23)$$

where ρ_b is the density of brine in (g/cm³), ρ_w is the density of fresh water which is assumed as 1 g/cm³ for fresh water, S is the salinity, T is the temperature that is given in Table-2.1 and P is pressure in GPa.

The velocity of brine water is computed as (Batzle and Wang, 1992):

$$V_b = V_w + S(1170 - 9.6T + 0.055T^2 - 8.5 \times 10^{-5}T^3 + 2.6P - 0.0029TP - 0.0476P^2) + S^{1.5}(780 - 10P + 0.16P^2) - 1820S^2 \quad (2.24)$$

V_b is the velocity of brine and V_w is the velocity of fresh water which is computed as (Batzle and Wang, 1992):

$$V_w = \sum_{i=0}^4 \sum_{j=0}^3 w_{ij} T^i P^j \quad (2.25)$$

where the coefficients w_{ij} are:

$$\begin{aligned} w_{00} &= 1402.85 & w_{02} &= 3.437 \times 10^{-3} \\ w_{10} &= 4.871 & w_{12} &= 1.739 \times 10^{-4} \\ w_{20} &= -0.04783 & w_{22} &= -2.135 \times 10^{-6} \\ w_{30} &= 1.487 \times 10^{-4} & w_{32} &= -1.455 \times 10^{-8} \\ w_{40} &= -2.197 \times 10^{-7} & w_{42} &= 5.230 \times 10^{-11} \\ w_{01} &= 1.524 & w_{03} &= -1.197 \times 10^{-5} \\ w_{11} &= -0.0111 & w_{13} &= -1628 \times 10^{-6} \\ w_{21} &= 2.747 \times 10^{-4} & w_{23} &= 1.237 \times 10^{-8} \\ w_{31} &= -6.503 \times 10^{-7} & w_{33} &= 1.327 \times 10^{-10} \\ w_{41} &= 7.987 \times 10^{-10} & w_{43} &= -4.614 \times 10^{-13} \end{aligned}$$

S is the salinity (ppm), P is the pressure (GPa), and temperature ($^{\circ}\text{C}$).

The bulk moduli of brine water is calculated as

$$K_b = (\rho * V_p) 10^{-6} \quad (2.26)$$

The computed properties of brine water are given in Table-2.4:

Table-2.4: Computed properties of brine water

S (PPM)	84000
ρ_b (g/cm^3)	1.059628
V_b (m/sec)	1499
K_b (Pascal)	2388227392

2.3 Matrix properties of reservoir

In this model, pure sandstone (i.e., clay content is zero) is assumed as reservoir rock. Using published data for bulk (K_m) and shear moduli (μ_m) of matrix, where K_m is 36.6 GPa and μ_m is 45 GPa (Mavko et. al).

2.4 Velocity and density model

For the computation of elastic properties such as the bulk modulus of the saturated rock (K_s), bulk modulus of dry rock (K_d) of Gassmann's equation, and saturated rock density, initially a velocity and density model is defined. The values of velocity and density are given in Table 2.5.

Table-2.5: Velocity and density model

First Layer	
V_p (m/sec)	3850
ρ_r (g/cm^3)	2.3
second Layer	
V_p (m/sec)	3344
ρ_r (g/cm^3)	2.317
Third Layer	
V_p (m/sec)	5140
ρ_r (g/cm^3)	2.5

2.5 Gassmann's equation for fluid substitution

Gassmann's equation is well known for fluid substitution to observe the seismic changes.

According to this equation, the bulk modulus of a saturated sedimentary rock is given as.

$$K_s = K_d + \frac{\left(1 - \frac{K_d}{K_m}\right)^2}{\frac{\phi}{K_f} + \frac{1-\phi}{K_m} - \frac{K_d}{K_m^2}} \quad (2.27)$$

where, K_s is the bulk modulus of the saturated rock, K_d is bulk modulus of dry rock, K_m bulk modulus of matrix of the rock, K_f is fluid bulk modulus and ϕ is porosity of the rock. K_m and ϕ are known to us. K_d and μ_d are computed using Nur et al. (1991, 1995) critical porosity equation as:

$$K_d = K_m \left(1 - \frac{\phi}{\phi_c}\right) \quad (2.28)$$

Similarly for μ_d

$$\mu_d = \mu_m \left(1 - \frac{\phi}{\phi_c}\right) \quad 2.29$$

K_m and μ_m are bulk and shear modulus of the mineral, which is in this case is quartz. \emptyset and \emptyset_c are porosity and critical porosity, respectively. Every rock type has its own critical porosity, and in this case, for sandstone, it is 0.4.

K_s is computed as:

$$K_s = K_d + \frac{(1 - K_d/K_m)^2}{\frac{\emptyset}{K_f} + \frac{1-\emptyset}{K_m} - \frac{K_d}{K_m^2}} \quad (2.30)$$

Saturated rock density is calculated using density-porosity equation, as given below:

$$\rho_s = (1 - \emptyset)\rho_m + \emptyset\rho_f \quad (2.31)$$

ρ_s , ρ_m and ρ_f are the saturated rock density, matrix density and fluid density in (g/cm^3) respectively and \emptyset is the porosity of reservoir rock.

Gassmann's equation is used for three different fluid substitutions: gas, live oil, and brine water at the reservoir level. This K_s is used to find the velocity of each fluid as:

$$V_p = \sqrt{\frac{K_s + 4/3\mu_s}{\rho_s}} \quad (2.32)$$

K_f is computed by the inversion of Gassmann's equation, as given below, as all the parameters of Gassmann's equation are known in the reservoir.

$$K_f = \frac{\emptyset(K_s - K_d)K_m^2}{[(K_m - K_d)(K_m - K_s) + (K_m * \emptyset)(K_s - K_d)]} \quad (2.33)$$

Tables 2.6 to 2.8 list the computed values for all the parameters of gas, live oil, and brine using the above equations, respectively..

Table 2.6: Computed parameters of reservoir fully saturated with gas

Gas	
ρ_s (g/cm ³)	2138.93
μ_d (Pascal)	$2.25 \cdot 10^{10}$
K_d (Pascal)	$1.8 \cdot 10^{10}$
K_s (Pascal)	$1.8 \cdot 10^{10}$
V_p (m/sec)	4737
K_o (Pascal)	219623.1432

Table-2.7: Computed parameters of reservoir fully saturated with live oil

Live Oil	
ρ_s (g/cm ³)	2264
μ_d (Pascal)	$2.25 \cdot 10^{10}$
K_d (Pascal)	$1.8 \cdot 10^{10}$
K_s (Pascal)	$1.849 \cdot 10^{10}$
V_p (m/sec)	4627
K_o (Pascal)	402040000

Table 2.8: Computed parameters of reservoir fully saturated with brine water

Brine Water	
ρ_s (g/cm ³)	2331
μ_d (Pascal)	2.25×10^{10}
K_d (Pascal)	1.8×10^{10}
K_s (Pascal)	2.07×10^{10}
V_p (m/sec)	4663
K_o (Pascal)	2.38×10^9

2.1 Fluid identification

Synthetic seismic data are generated for the above geological model using the convolution method, which will be discussed in the next chapter. In this model, the surface to the top of the second layer is assumed as one layer with an average velocity V_p of 3850 m/s and density of 2.3 g/cm³. The second layer is a cap shale rock with its top at 1600 m and bottom at 2000 m. The thickness of the cap rock is 400 m, its average velocity (V_p) is 3344 m/s, and its density is 2.317 g/cm³. The third layer is the reservoir formation, which is pure sandstone with its crest at 2000 m and dipping down to 3000 m. The maximum thickness of the hydrocarbon column is 200 m, whereas the remaining part of the reservoir is fully saturated with brine water. The water-saturated part of the reservoir has a velocity (V_p) of 4663 m/s and a density of 2.331 g/cm³, whereas, in the hydrocarbon column, in the case of live oil, the velocity is 4627 m/s and the density is 2.264 g/cm³ and, in case of gas, the velocity is 4737 m/s and the density is 2.138 g/cm³. For fluid substitution, there are two cases:

- i. Gas present at the top of the reservoir, which is followed by brine water, and
- ii. Live oil present at the top of the reservoir, which is followed by brine water.

Saturated rock bulk density (ρ_s) and velocity(V_p) are computed using the above equations, with values given in Tables 2.9 to 2.11.

Using the computed velocities and densities of each layer of the model, synthetic seismic data are generated for both cases. From these seismic data, AI and stacking velocity data will be calculated. Dix's equation will be used to compute the interval velocity:

$$V_{intN} = \sqrt{\frac{V_{RMSN}^2 T(O)_N - V_{RMSN-1}^2 T(O)_{N-1}}{T(O)_N - T(O)_{N-1}}} \quad (2.34)$$

where, V_{intN} is the interval velocity of the N^{th} , V_{RMSN} is the RMS velocity of the N^{th} layer and V_{RMSN-1} is the RMS velocity of layer just above the N^{th} .

AI is the product of acoustic velocity and density. For AI inversion, I used the recursive inversion method using the following formula:

$$Z_{i+1} = Z_1 \frac{1+k_i}{1-k_i} \quad 2.35$$

Z_1 is the AI of the first layer, which is assumed to be known. The RC of each layer is computed using deconvolution of the seismic data.

$$RC = \frac{V_2 \rho_2 - V_1 \rho_1}{V_2 \rho_2 + V_1 \rho_1} \quad 2.36$$

where RC is the reflection coefficient, V_1 and V_2 are the velocities of the first and second layer, ρ_1 and ρ_2 are densities of the first and layer second layer respectively.

Z_1 is computed using P-wave velocity and density of the first layer. I computed the compressional modulus using following equation:

$$V_p^2 * \rho_s = V_p * AI = M \quad (2.37)$$

V_p is the interval P-wave velocity, AI is the acoustic impedance, computed from seismic data and M is the compressional modulus of saturated rock.

The computed interval velocity and AI are inverted into fluid velocity and density as:

For the density of the fluid, the density-porosity equation of density log is inverted as:

$$\rho_f = \frac{\rho_s - (1 - \emptyset) * \rho_m}{\emptyset} \quad (2.38)$$

ρ_f is the density of the fluid in the reservoir, ρ_m is the density of matrix, \emptyset is the porosity of reservoir and ρ_s is the density of saturated rock which is calculated as:

$$\rho_s = \frac{AI}{V_p} \quad (2.39)$$

ρ_s is the saturated rock density in Kg/m^3 , AI is the acoustic impedance computed from surface seismic data and V_p is the P-wave velocity also estimated from surface seismic data.

The velocity of the fluid is computed as:

$$V_f = \sqrt{\frac{K_f}{\rho_f}} \quad (2.40)$$

Where, V_f is the fluid velocity in m/sec, K_f is the fluid bulk modulus and ρ_f is the fluid density.

CHAPTER 3

SEISMIC DATA GENERATION

3.1 Synthetic seismogram

For this model, the synthetic seismic data are generated using the convolutional model of the seismic trace (Yilmaz, 2001). Using following steps, I generated the synthetic seismogram for each case. First, I computed the AI using the velocity and density of each layer, which I have obtained from the density and velocity model for each sample using the following equation:

$$AI = V_p * \rho \quad 3.1$$

- ✓ Then, the RC is computed using those AI values of each sample using the following equation:

$$RC = \frac{V_2\rho_2 - V_1\rho_1}{V_2\rho_2 + V_1\rho_1} \quad 3.2$$

- ✓ Finally, I chose a suitable wavelet, which is, in this case, a minimum phase wavelet and convolved it with the whole RC series and generated the synthetic seismogram.

3.1.1 Case-1

Figure 3.1 shows the RC plot of case 1, in which gas is present at the top of the reservoir followed by brine. Along the x -axis is RC, which ranges from -0.1 to 0.15, whereas the y -axis is time ranging from 0 to 1.5 s.

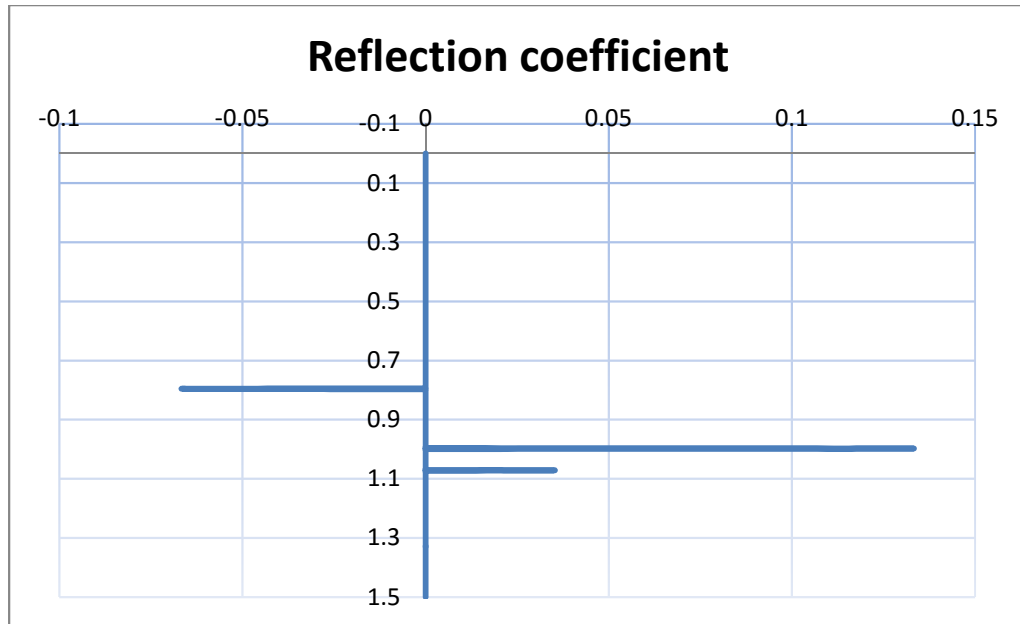


Figure 3.1: Reflection coefficient plot of case-1

The RC of the first reflector is -0.06667 at 0.8 s, which is between sandstone and shale.

The RC of the second reflector is 0.1333 at 0.99 s, which is between shale and sandstone.

The RC of the third reflector is 0.03533 at 1.07 s, which is between the gas-saturated zone and the brine-saturated zone.

Figure 3.2 shows the minimum phase wavelet, where the x -axis is time, whereas the y -axis is the amplitude of the wavelet. The maximum amplitude of the wavelet is 1 at about 0.005 s.

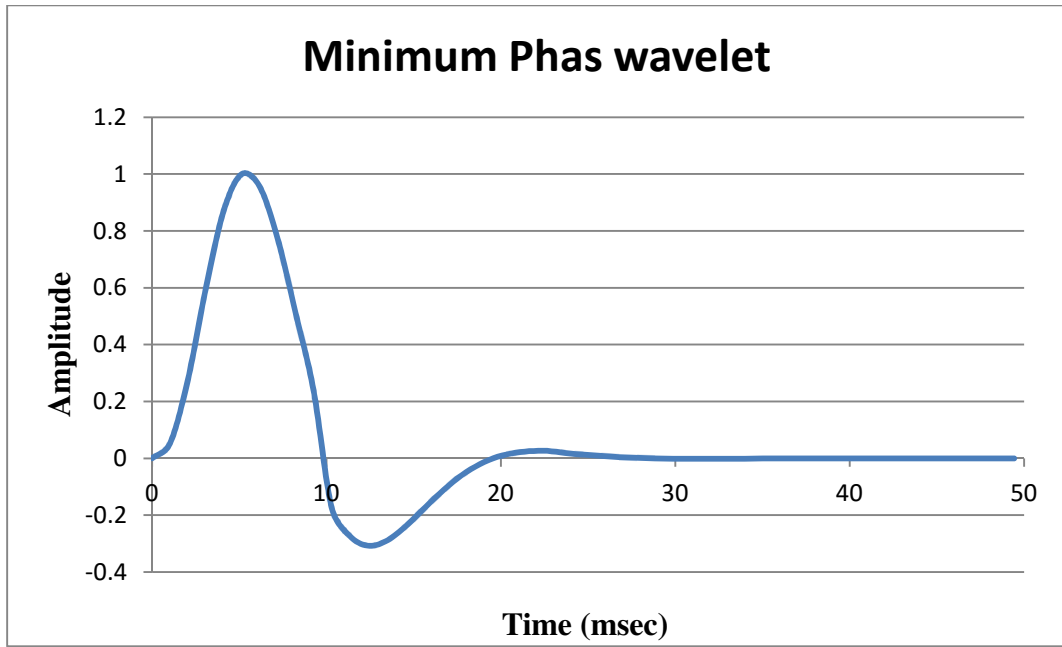


Figure 3.2: Minimum phase wavelet plot

Figure 3.3 shows the trace resulting from the convolution of the above minimum phase wavelet with the RC series.

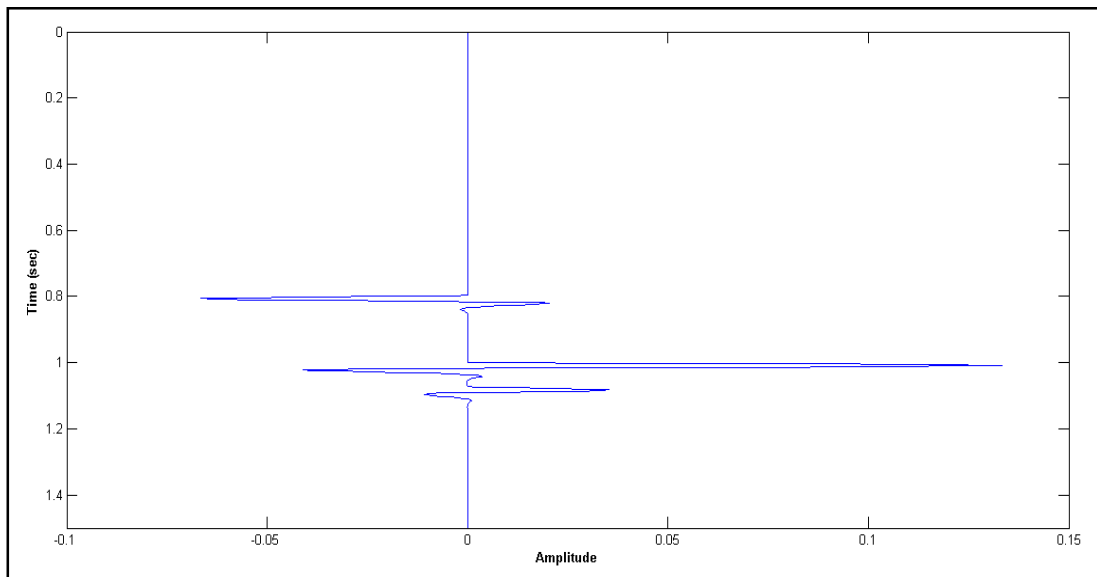


Figure 3.3: Trace of case-1

3.1.2 Case-2

Figure 3.4 shows the RC plot of case 2, in which live oil is present at the top of the reservoir and followed by brine. The RC ranges from -0.1 to 0.2, whereas time ranges from 0 to 1.5 s.

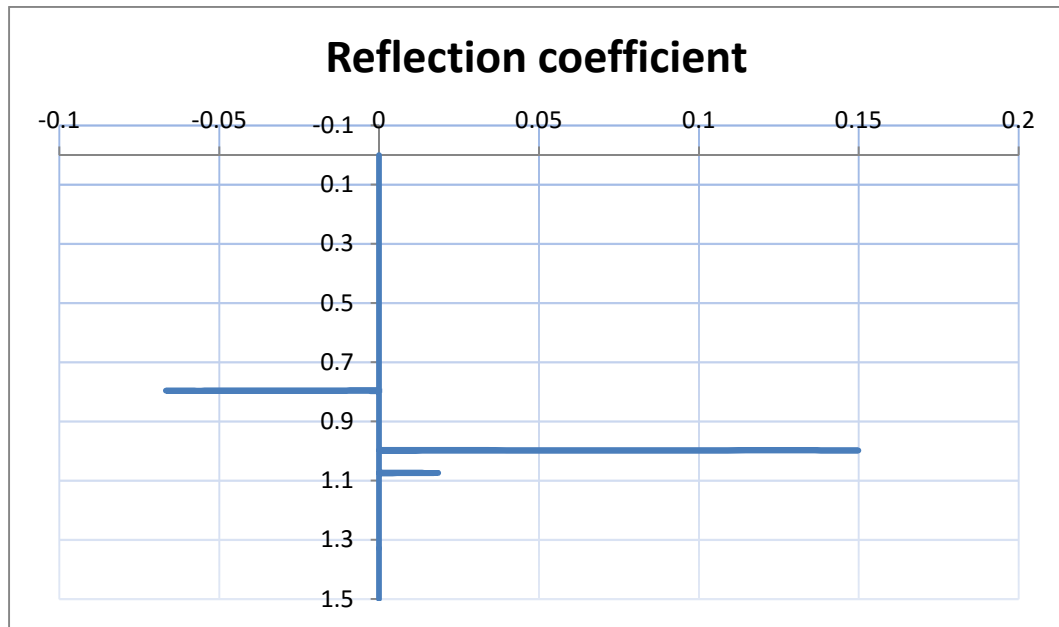


Figure 3.4: Reflection coefficient plot of case-2

The RC of the first reflector is -0.06667 at 0.8 s, which is between sandstone and shale. The RC of the second reflector is 0.15 at 0.99 s, which is between shale and sandstone. The RC of the third reflector is 0.0185 at 1.07 s, which is between the gas-saturated zone and the brine-saturated zone.

Figure 3.5 shows the trace in the resulting from the convolution of the above minimum phase wavelet with the RC series.

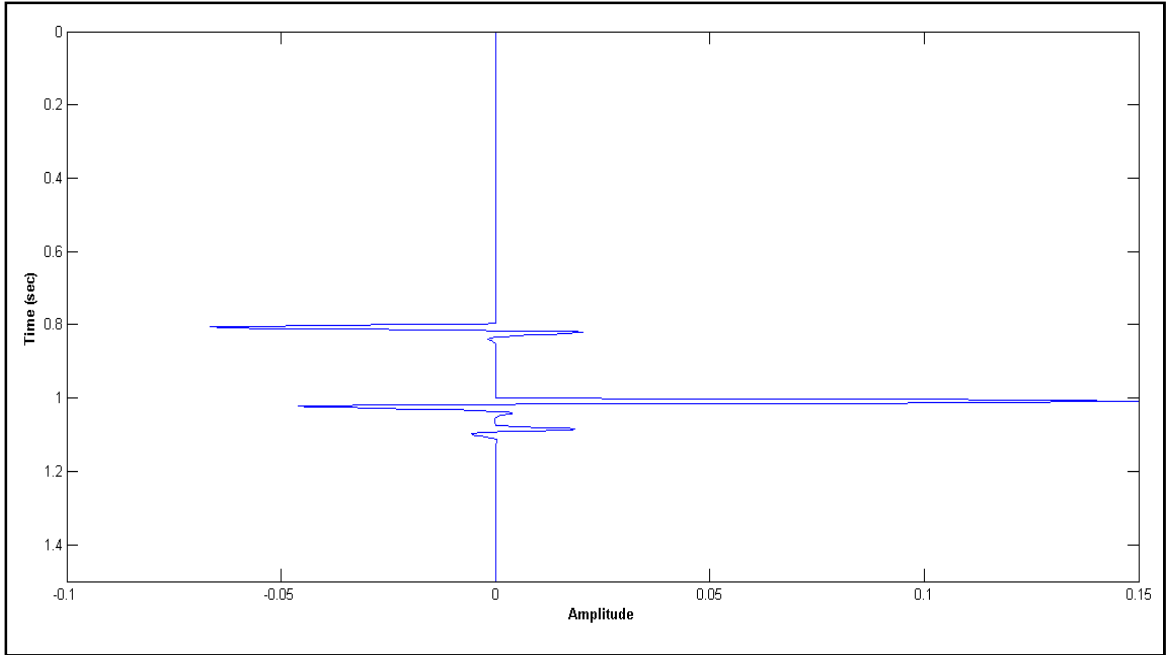


Figure 3.5: Trace of case-2

CHAPTER 4

RESULTS AND DISCUSSION

In the first case, the upper portion of the reservoir is fully saturated with gas, which is followed by brine water. In the second case, the uppermost part is saturated with live oil, which is followed by brine water. For both cases, AI, compressional modulus, fluid density, and fluid velocity inversion have been used to identify the pore fluid in the reservoir.

4.1 Case-1

4.1.1 AI inversion

Figure 4.1 shows the AI plot of the trace, which is exactly in the middle of the model as well as of the reservoir. From 0 to 0.8 s, AI remains the same for the first layer, which is sandstone. Then, it starts to increase from 0.8 to 1 s for the cap rock (shale). As we enter into the reservoir, which is pure sandstone, AI starts to increase from 1 to 1.07 s and the AI reaches up to $1.0133 * 10^7 \text{ kg s/m}^2$. After 1.07 s, there is a sudden change in AI and it starts to increase again and goes up to $1.08749 * 10^7 \text{ kg s/m}^2$ (7.3%).

Based on AI inversion, we can separate the upper part of the reservoir, which is from 1 to 1.07 s, from the lower part, which is from 1.07 to 1.5 s. This is the evidence that there are two different pore fluids present in the reservoir.

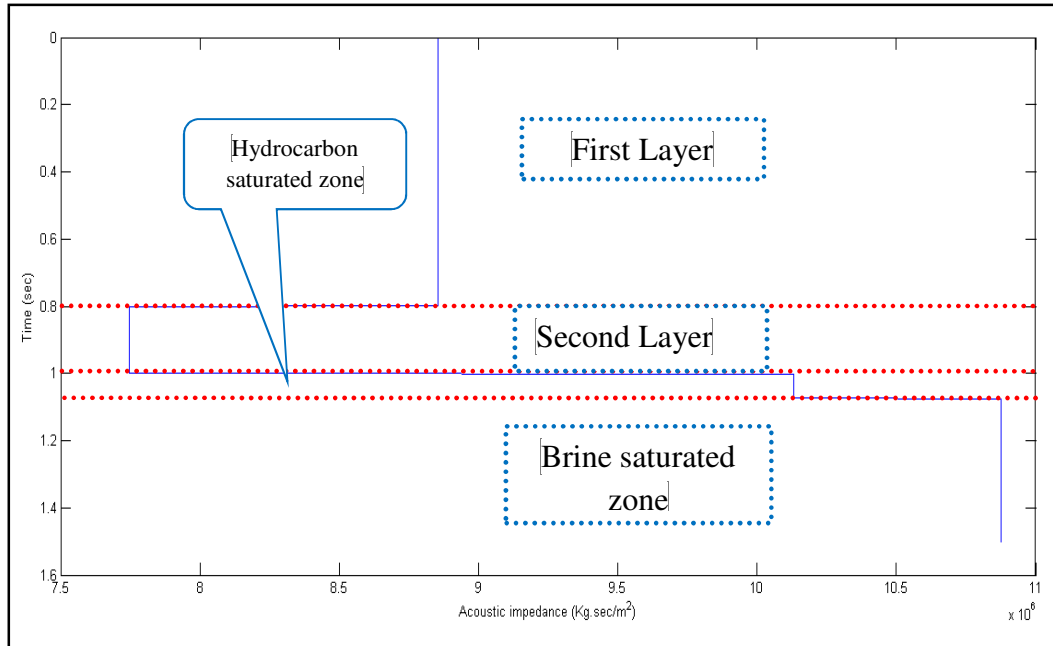


Figure 4.1: Acoustic impedance plot of case-1

4.1.2 Compressional modulus (M)

Figure-4.2 shows the compressional bulk modulus (M) plot of the trace which is exactly in the middle of the model as well as of the reservoir. From 0 to 0.8 s, M remains the same for the first layer, which is sandstone. Then, it starts to increase from 0.8 to 1 s for the cap rock (shale). As we enter into the reservoir, M starts to increase from 1 sec up to 1.07 sec and reaches up to $4.8 * 10^{10}$ Pascal. After 1.07 sec, there is a sudden change in M and it starts to increase again and goes up to $5.072 * 10^{10}$ Pascal (5.7%).

Based on M inversion, we can separate the upper part of the reservoir, which is from 1 to 1.07 s, from the lower part, which is from 1.07 to 1.5 s. This is also the evidence that there are two different pore fluids present in the reservoir.

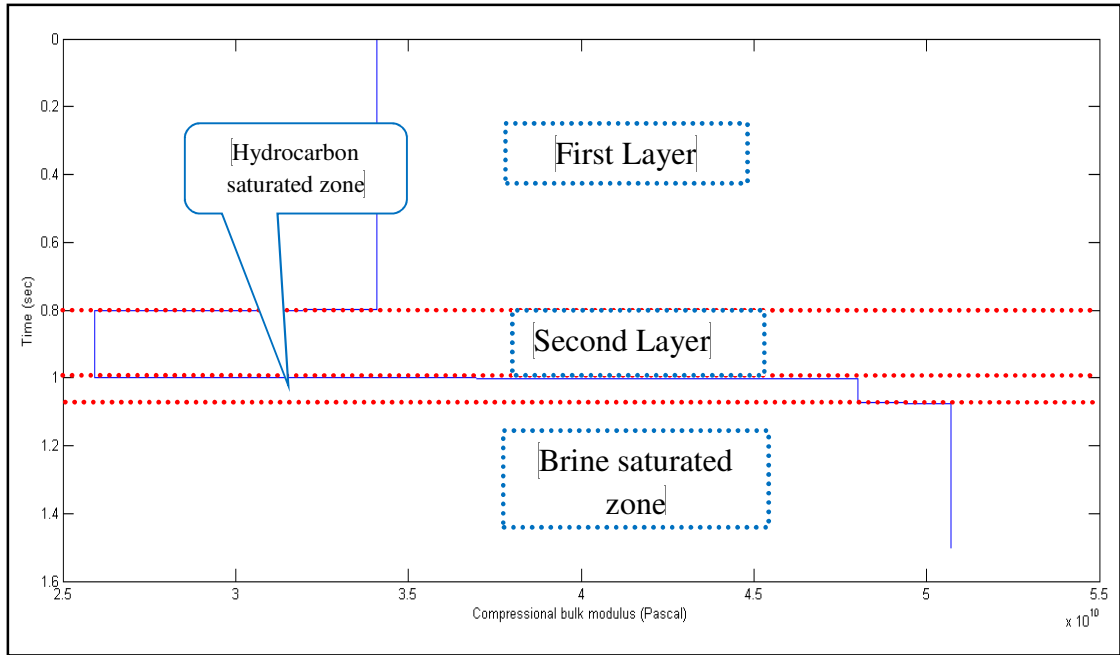


Figure 4.2: Compressional bulk modulus plot of case-1

4.1.3 Saturated rock density (ρ_s)

Figure-4.3 shows the saturated rock density (ρ_s) plot of the trace which is exactly in the middle of the model as well as of the reservoir. From 0 to 0.8 s ρ_s remains the same for the first layer which is sandstone. Then, it starts to increase from 0.8 to 1 s for the cap rock (shale), as the second layer has high density compared to the first layer. As we enter into the reservoir, ρ_s starts to decrease from 1 to 1.07 s and the ρ_s reach down to 2138 Kg/m^3 . After 1.07 s, there is a sudden change in ρ_s and it starts to increase again and goes up to 2331 Kg/m^3 (9.03%).

Based on ρ_s inversion, we can separate the upper part of the reservoir, which is from 1 to 1.07 s (it has low saturated rock density), from the lower part, which is from 1.07 to 1.5 s (it has high saturated rock density). This is also the evidence that there are two different pore fluids present in the reservoir due to which we have two different saturated rock densities in the same reservoir..

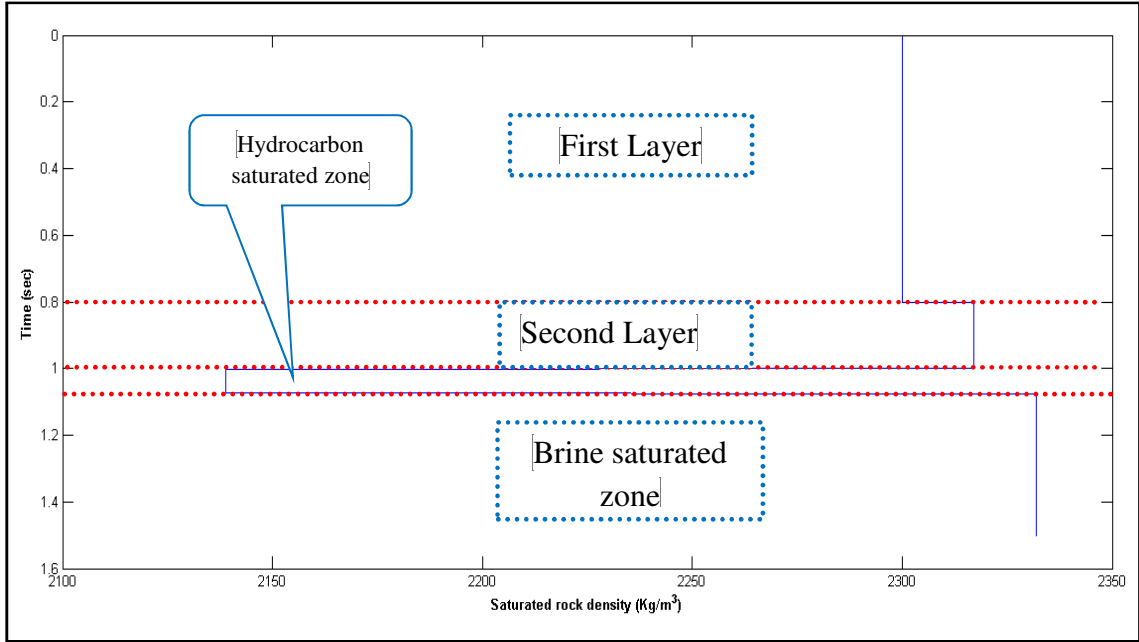


Figure 4.3: Saturated rock density plot of case-1

4.1.4 Fluid density (ρ_f)

Figure-4.4 shows the fluid density (ρ_f) plot of the trace which is exactly in the middle of the model as well as of the reservoir. From 0 sec to 1 sec ρ_f has no value because we don't have any fluid in upper two layers. As we enter into reservoir, ρ_f starts to increase from 0 to 95 Kg/m^3 . Between 1 sec up to 1.07 sec ρ_f remains the same at 95 Kg/m^3 . After 1.07 sec, there is a sudden change in ρ_f and it starts to increase again and goes up to 1059 Kg/m^3 (1014.74%).

Based on ρ_f inversion and the range of fluid densities in the reservoir, we can easily identify pore fluid in the reservoir. The upper part, which is from 1 to 1.07 s, is the gas saturated zone because of the fluid density in this zone is 95 Kg/m^3 . Whereas the lower part, which is from 1.07 to 1.5 s is the brine saturated zone because the fluid density in this zone is 1059 Kg/m^3 .

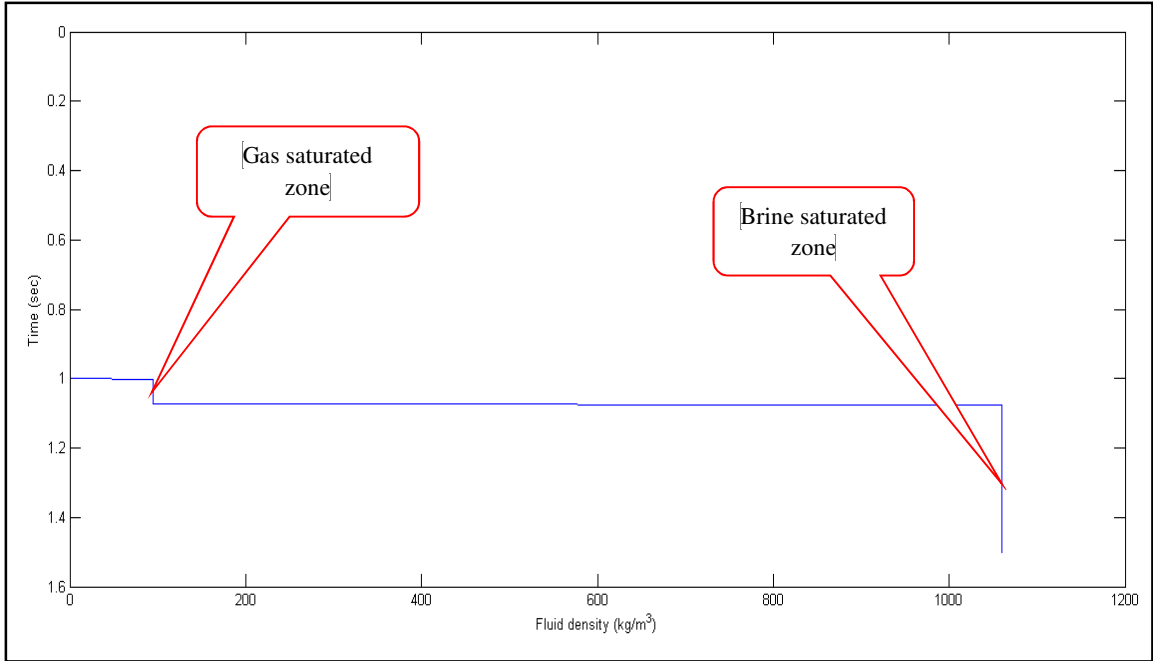


Figure 4.4: Fluid density plot of case-1

4.1.5 Fluid velocity (V_f)

Figure-4.5 shows the fluid velocity (V_f) plot of the trace which is exactly in the middle of the model as well as of the reservoir. V_f has no value because we do not have any fluid in the upper two layers. As we enter into the reservoir, V_f starts to increase from 0 to 50 m/s, between 1 and 1.07 s and the V_f remains the same at 50 m/s. After 1.07 s, then there is a sudden change in V_f and it starts to increase again and goes up to 1500 m/s (2900%).

Based on V_f inversion and the range of fluid velocities in the reservoir, we can easily identify pore fluid in the reservoir. The upper part, which is from 1 to 1.07 s, is the gas-saturated zone because the fluid velocity in this zone is 50 m/s, whereas the lower part, which is from 1.07 to 1.5 s is the brine-saturated zone because the fluid velocity in this zone is 1500 m/s.

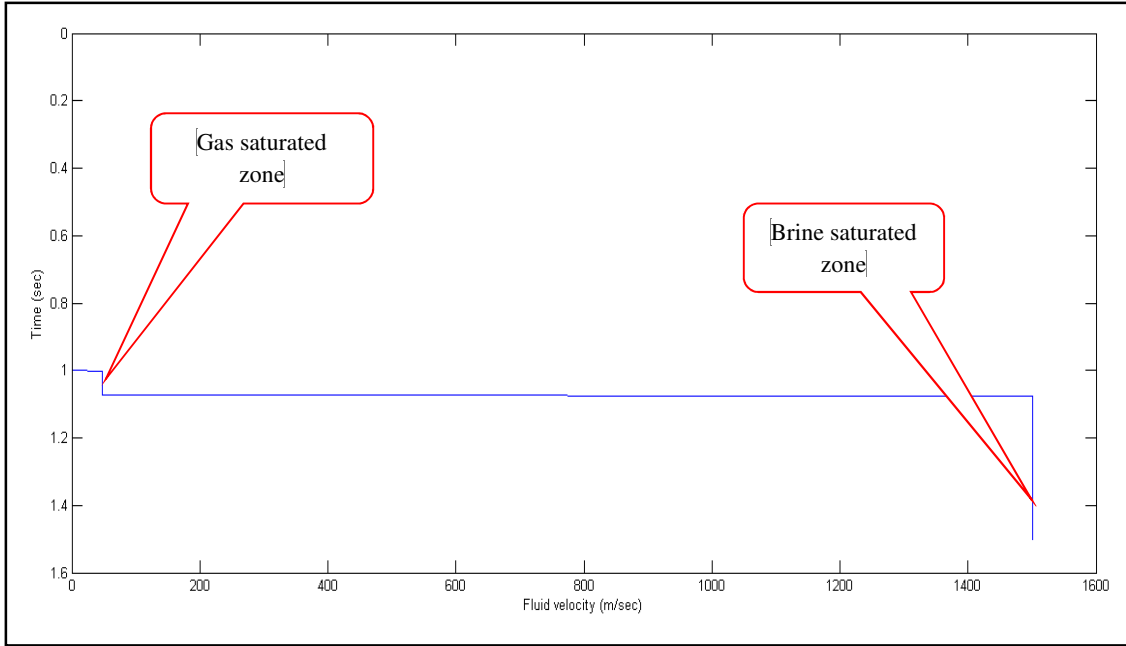


Figure 4.5: Fluid velocity plot of case-1

4.2 Case-2

4.2.1 AI inversion

Figure-4.6 shows the AI plot of the trace, which is exactly in the middle of the model as well as of the reservoir. From 0 to 0.8 s, AI remains the same for the first layer, which is sandstone. Then, it starts to increase from 0.8 to 1 s for the cap rock (shale). As we enter into the reservoir, which is pure sandstone, AI starts to increase from 1 to 1.07 s and the AI reaches up to $1.0479 * 10^7 \text{ Kg. sec/m}^2$. After 1.07 sec, there is a sudden change in AI and it starts to increase again and goes up to $1.08749 * 10^7 \text{ Kg. sec/m}^2$ (3.8%).

Based on AI inversion, we can separate the upper part of the reservoir, which is from 1 to 1.07 s, from the lower part, which is from 1.07 to 1.5 s. This is the evidence that there are two different pore fluids present in the reservoir.

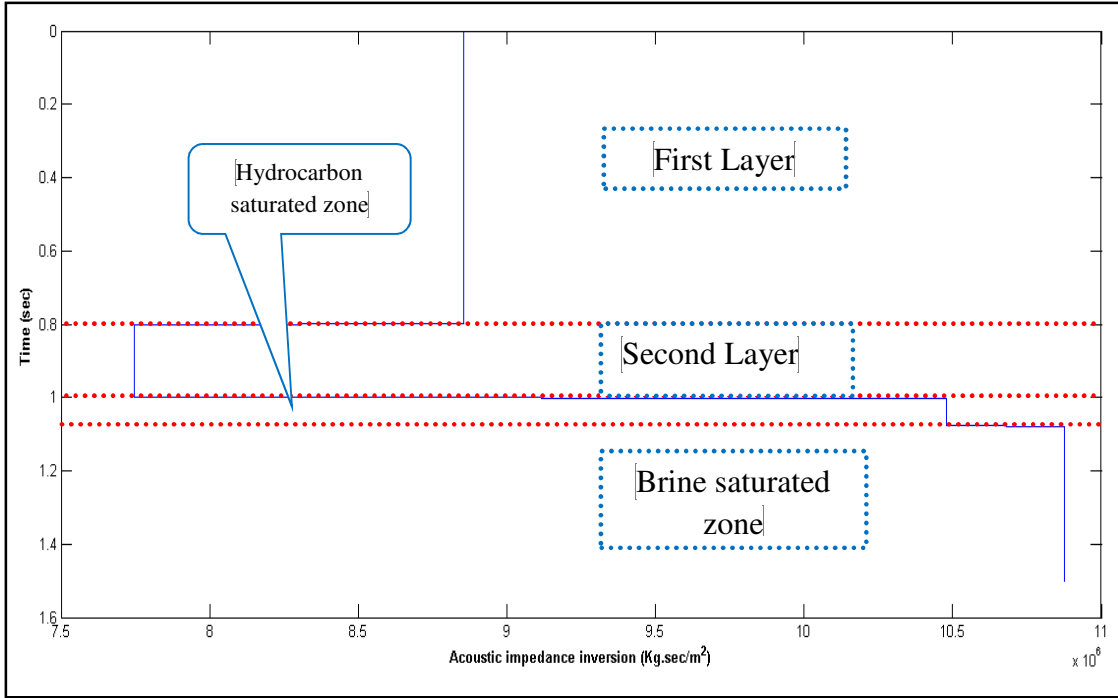


Figure 4.6: Acoustic impedance plot of case-2

4.2.2 Compressional modulus (M)

Figure 4.7 shows the compressional bulk modulus (M) plot of the trace, which is exactly in the middle of the model as well as of the reservoir. From 0 to 0.8 s, M remains the same for the first layer, which is sandstone. Then, it starts to increase from 0.8 to 1 s for the cap rock (shale). As we enter into the reservoir, M starts to increase from 1 sec up to 1.07 sec and reaches up to $4.849 * 10^{10}$ Pascal. After 1.07 s, there is a sudden change in M and it starts to increase again and goes up to $5.072 * 10^{10}$ Pascal (4.6%).

Based on M inversion, we can separate the upper part of the reservoir, which is from 1 to 1.07 s, from the lower part, which is from 1.07 to 1.5 s. This is also the evidence that there are two different pore fluids present in the reservoir.

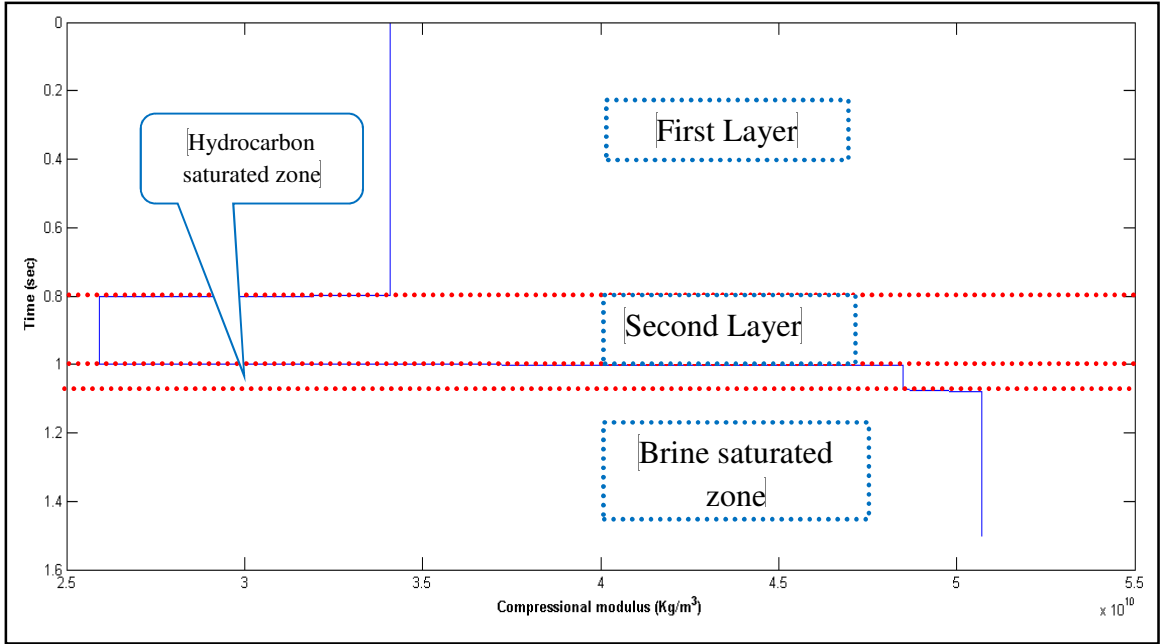


Figure 4.7: Compressional modulus plot of case-2

4.2.3 Saturated rock density (ρ_s)

Figure-4.8 shows the saturated rock density (ρ_s) plot of the trace, which is exactly in the middle of the model as well as of the reservoir. From 0 to 0.8 s ρ_s remains the same for the first layer, which is sandstone. Then, it starts to increase from 0.8 to 1 s for the cap rock (shale), as the second layer has high density compared to the first layer. As we enter into the reservoir, ρ_s starts to decrease from 1 sec up to 1.07 sec and the ρ_s reaches down to 2264 Kg/m^3 . After 1.07 sec, there is a sudden change in ρ_s and it starts to increase again and goes up to 2331 Kg/m^3 (3%).

Based on ρ_s inversion, we can separate the upper part of the reservoir, which is from 1 to 1.07 s (it has low saturated rock density), from the lower part, which is from 1.07 to 1.5 s (it has high saturated rock density). This is also the evidence that there are two different pore fluids present in the reservoir due to which we have two different saturated rock densities in the same reservoir.

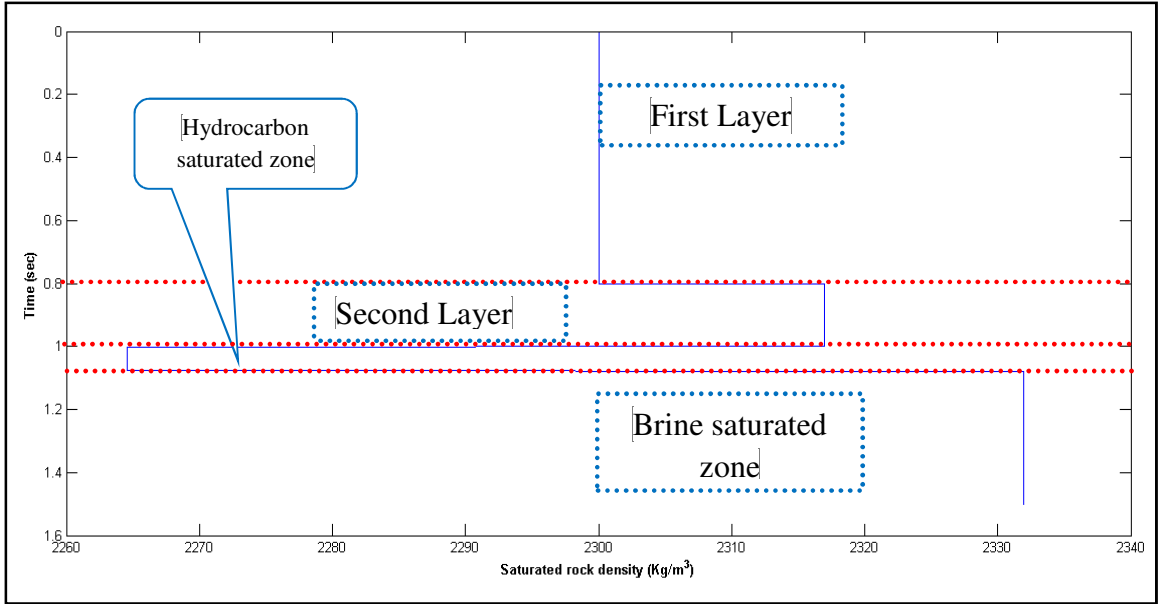


Figure 4.8: Saturated rock density plot of case-2

4.2.4 Fluid density (ρ_f)

Figure-4.9 shows the fluid density (ρ_f) plot of the trace, which is exactly in the middle of the model as well as of the reservoir. From 0 to 1 ρ_f has no value because we do not have any fluid in the upper two layers. As we enter into the reservoir, ρ_f starts to increase from 0 to 722 Kg/m^3 . Between 1 to 1.07 s and the ρ_f remains the same at 722 Kg/m^3 . After 1.07 s, there is a sudden change in ρ_f and it starts to increase again and goes up to 1059 Kg/m^3 (46.7%).

Based on ρ_f inversion and the range of fluid densities in the reservoir, we can easily identify pore fluid in the reservoir. The upper part, which is from 1 to 1.07 s, is the oil saturated zone because the fluid density in this zone is 722 Kg/m^3 . Whereas the lower part, which is from 1.07 to 1.5 s, is the brine is 1059 Kg/m^3 .

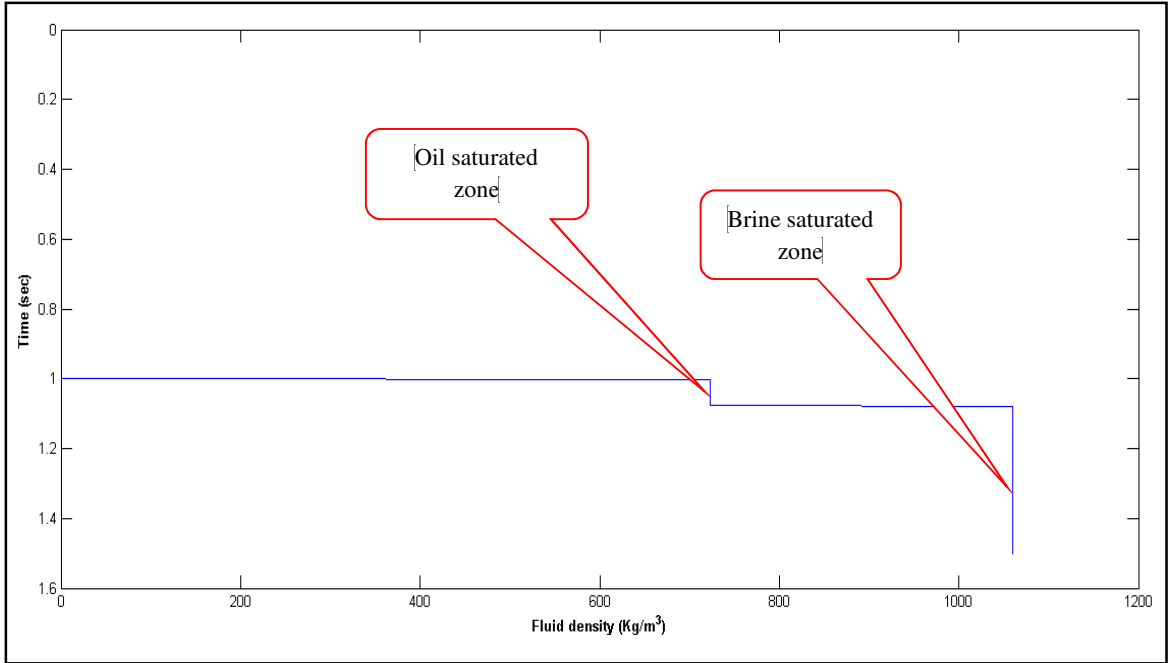


Figure 4.9: Fluid density plot of case-2

4.2.5 Fluid velocity (V_f)

Figure-4.10 shows the fluid velocity (V_f) plot of the trace, which is exactly in the middle of the model as well as of the reservoir. From 0 to 1 s V_f has no value because we do not have any fluid in the upper two layers. As we enter into the reservoir, V_f starts to increase from 0 to 745 m/sec, between 1 and 1.07 s the V_f remains the same at 745 m/sec. After 1.07 s, there is a sudden change in V_f and it starts to increase again and goes up to 1500 m/sec (101.3%).

Based on V_f inversion and the range of fluid velocities in the reservoir, we can easily identify pore fluid in the reservoir. The upper part, which is from 1 to 1.07 s, is the oil-saturated zone because the fluid velocity in this zone is 745 m/s, whereas the lower part, which is from 1.07 to 1.5 s, is the brine-saturated zone because the fluid velocity in this zone is 1500 m/s.

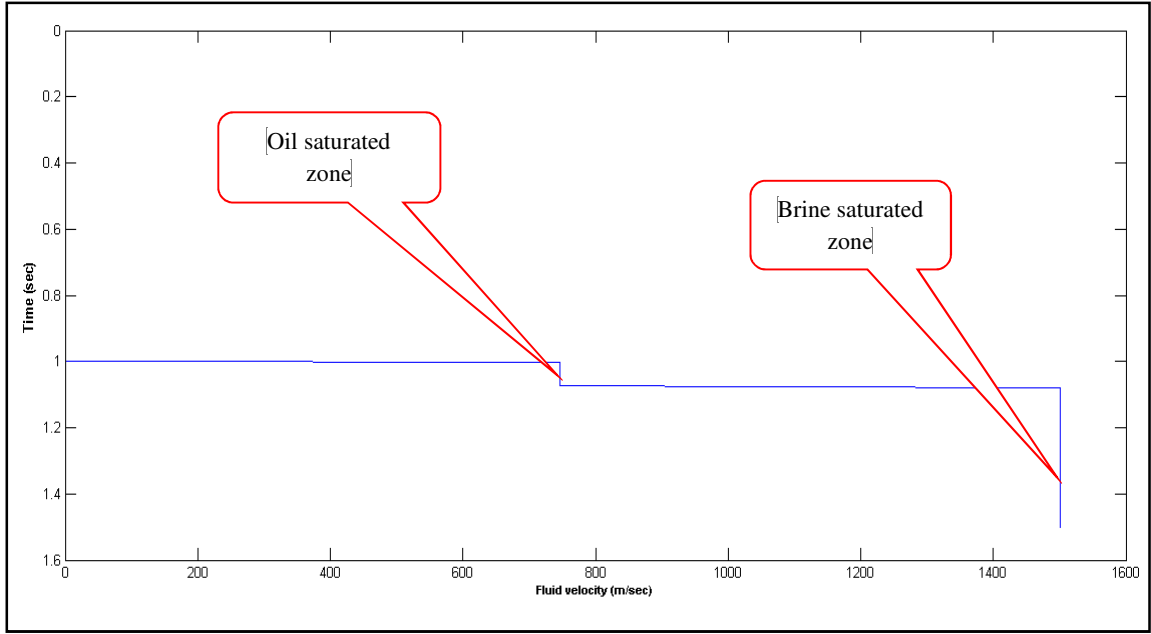


Figure 4.10: Fluid velocity plot of case-2

4.3 Case-3

In the previous two cases, the algorithm worked very well. The only constraint is porosity, which we assumed for the model and was not computed by any means. In case 3, the proposed model will be applied using the published porosity data of the Arab formation.

Steineke (1937) assigned the Arab formation as a part of Riyadh members (Powers et al., 1966). Steineke (1958) assigned this formation as the Arab formation. The type locality of the Arab formation was selected near Riyadh City but, due to the extensive erosion and weathering, only the subsurface section was assumed the best representation of the Arab formation (Powers et al., 1966). The base contact of the Arab formation is with Jubaila limestone, whereas the top contact is with Hith anhydrite. The Arab formation is further divided into four members, which are A, B, C, and D. Although all the members have hydrocarbon potential, Arab D is more prolific. Hith anhydrite provides the seal for the Arab formation.

The Ghawar oil field is an anticline structure with approximately 200 km length and 16 km width. The porosity of the Arab formation is either primary porosity or due to the early diagenetic secondary porosity. The porosity is different in different members of the Arab formation. Wilson (1981) investigated the porosity in Arab C and Arab D members and found that the porosity ranged from 1% to 30%.

In this case study, the live-oil case with porosity ranging from 10% to 30% with 10% interval has been studied. Tables 4.1 to 4.3 give the assumed parameters, the live-oil computed properties, and the brine computed properties of Arab reservoir, respectively.

Table 4.1: Assumed parameters of Arab formation

Porosity	Reservoir porosity	10-30%
T (°C)	Temperature at reservoir level	150
Depth (m)	Reservoir depth at crest	1600

Table 4.2: Live oil properties for the Arab formation

G	0.56
P (GPa)	0.0212
R_g	0.0237
B_o (bbl/STB)	1.1283
ρ' (g/cm ³)	0.7228
ρ_g (g/cm ³)	0.7228
ρ_p (g/cm ³)	0.7229
V_p (m/sec)	745.7754
K_o (Pascal)	402040000

Table 4.3: Brine properties for the Arab formation

S (PPM)	84000
ρ_b (g/cm ³)	1.059628
V_b (m/sec)	1499
K_b (Pascal)	2388227392

4.4 Matrix properties of reservoir

For the Arab formation, pure limestone is assumed as reservoir rock with a range of 10-30% porosity with matrix density 2.71 g/cm^3 and using the published data for matrix bulk (K_m) and shear moduli (μ_m), where K_m is 76.8 GPa and μ_m is 32 GPa (Mavko et. al).

4.5 Velocity and density model

For the computation of elastic properties such as the bulk modulus of the saturated rock (K_s), bulk modulus of dry rock (K_d) of Gassmann's equation, and saturated rock density, initially a velocity and density model is defined. The values of velocity and density are given in Table-4.4.

Table 4.4: Velocity and density model for Arab formation

First Layer	
V_p (m/sec)	3850
ρ_r (g/cm^3)	2.3
second Layer	
V_p (m/sec)	3344
ρ_r (g/cm^3)	2.317
Third Layer	
V_p (m/sec)	5140
ρ_r (g/cm^3)	2.4

4.6 10% Porosity

4.6.1 Fluid density (ρ_f)

Figure-4.11 shows the fluid density plot of the trace, which is exactly in the middle of the model as well as of the reservoir. To study the effect on fluid density in this case, the porosity of the Arab formation is assumed to be 10%. From 0 to 1 s, ρ_f has no value because we do not have any fluid in the upper two layers. As we enter into reservoir, ρ_f starts to increase from 0 to 723 Kg/m^3 . Between 1 to 1.07 s the ρ_f remains at 723 Kg/m^3 . After 1.07 s, there is a sudden change in ρ_f and it starts to increase again and goes up to 1062 Kg/m^3 (46.9%).

Based on ρ_f inversion and the range of fluid densities in the reservoir, we can easily identify pore fluid in the reservoir. The upper part, which is from 1 to 1.07 s, is the oil saturated zone because the fluid density in this zone is 723 whereas the lower part, which is from 1.07 to 1.5 s, is the brine saturated zone with 1062 Kg/m^3 density.

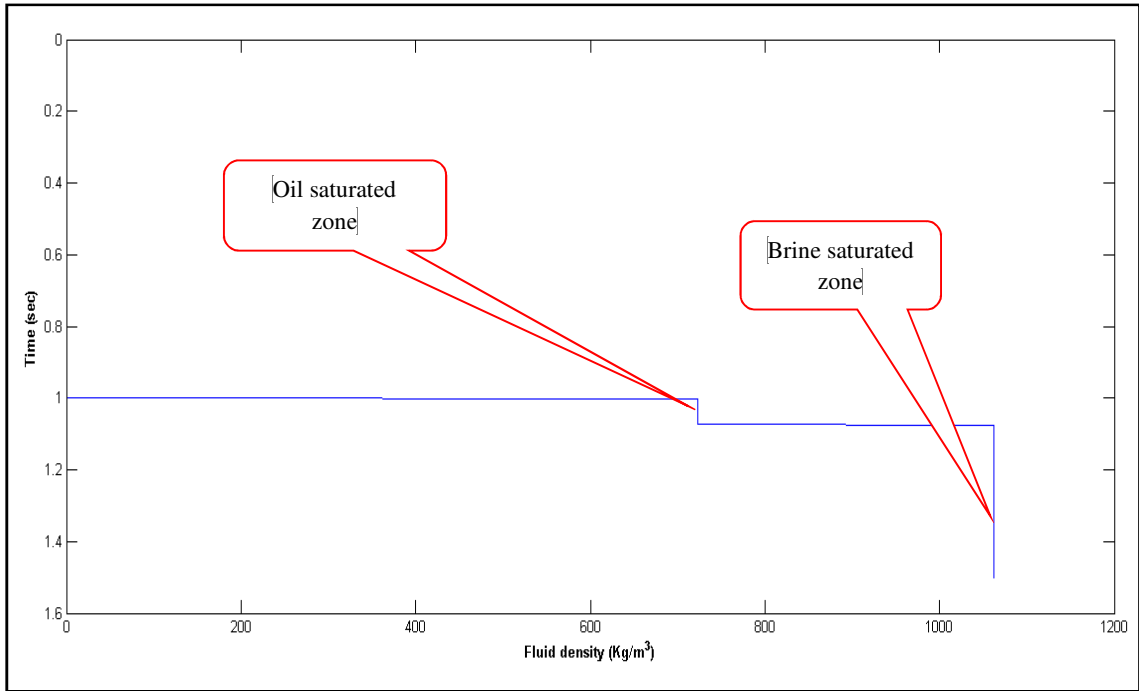


Figure 4.11: Fluid density plot with 10% porosity of Arab formation

4.6.2 Fluid velocity (V_f)

Figure-4.12 shows the fluid velocity (V_f) plot of the trace, which is exactly in the middle of the model as well as of the reservoir. In this case, the porosity of the Arab formation is assumed to be 10% to observe the effect on fluid velocity. From 0 to 1 s, V_f has no value because we do not have any fluid in the upper two layers. As we enter into the reservoir, V_f starts to increase from 0 to 746 m/sec, between 1 and 1.07 s the V_f remains at 746 m/sec. After 1.07 sec, there is a sudden change in V_f and it starts to increase again and goes up to 1481 m/sec (98.5%).

Based on V_f inversion and the range of fluid velocities in the reservoir, we can easily identify pore fluid in the reservoir. The upper part, which is from 1 to 1.07 s, is the oil-saturated zone because the fluid velocity in this zone is 746 m/s, whereas the lower part, which is from 1.07 to 1.5 s, is the brine-saturated zone because the fluid velocity in this zone is 1481 m/s.

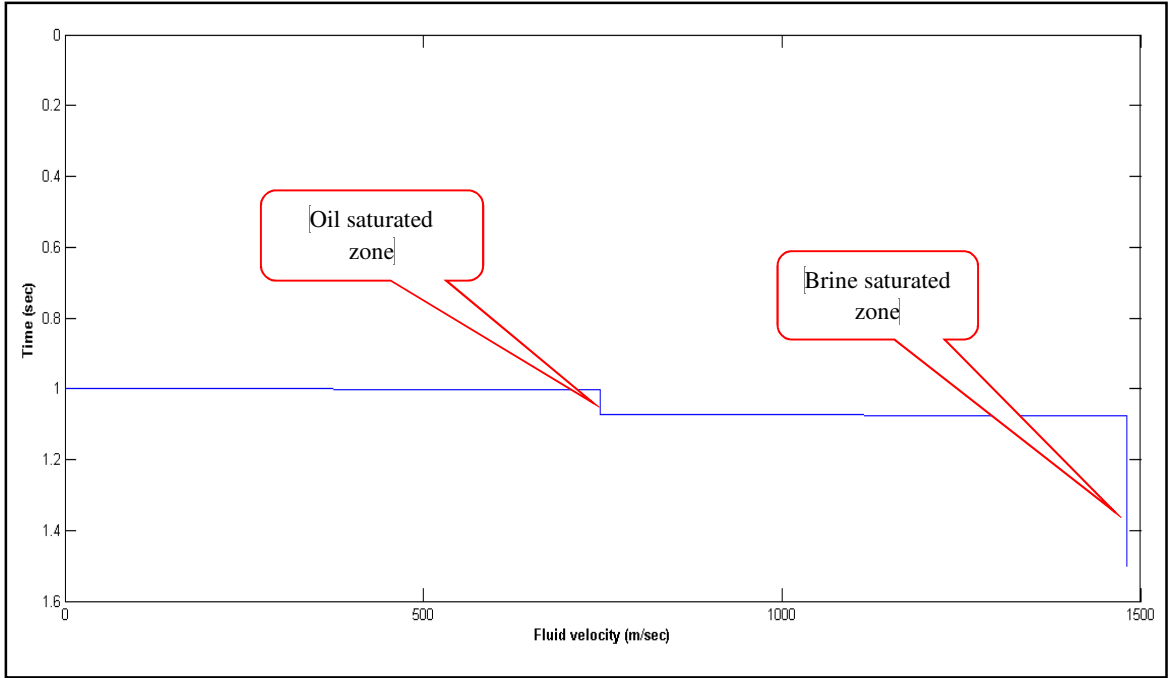


Figure 4.12: Fluid velocity plot with 10% porosity of Arab formation

4.7 20% Porosity

4.7.1 Fluid density (ρ_f)

Figure-4.13 shows the fluid density (ρ_f) plot of the trace, which is exactly in the middle of the model as well as of the reservoir. In this case, the porosity of the Arab formation is assumed to be 20% to observe the effect on fluid density. From 0 sec to 1 sec ρ_f has no value because we do not have any fluid in the upper two layers. As we enter into the reservoir, ρ_f starts to increase from 0 to 723 Kg/m^3 . Between 1 to 1.07 s and the ρ_f remains at 723 Kg/m^3 . After 1.07 s, there is a sudden change in ρ_f and it starts to increase again and goes up to 1062 Kg/m^3 (46.9%).

Based on ρ_f inversion and the range of fluid densities in the reservoir, we can easily identify pore fluid in the reservoir. The upper part, which is from 1 to 1.07 s, is the oil saturated zone because the fluid density in this zone is 723 Kg/m^3 , whereas the lower part, which is from 1.07 to 1.5 s, is the brine saturated zone with 1062 Kg/m^3 density.

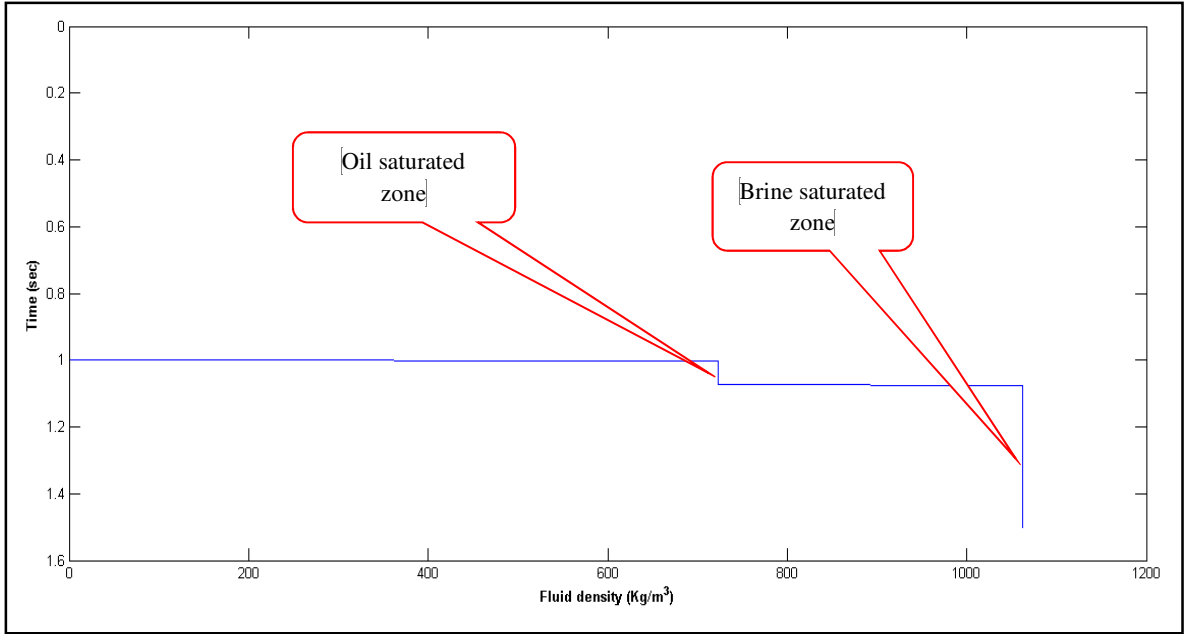


Figure 4.13: Fluid density plot with 20% porosity of Arab formation

4.7.2 Fluid velocity (V_f)

Figure-4.14 shows the fluid velocity (V_f) plot of the trace, which is exactly in the middle of the model as well as of the reservoir. In this case, the porosity of the Arab formation is assumed to be 20% to observe the effect on fluid velocity. From 0 to 1 s V_f has no value because we do not have any fluid in the upper two layers. As we enter into the reservoir, V_f starts to increase from 0 to 745 m/sec, between 1 and 1.07 s the V_f remains at 745 m/sec. After 1.07 s, there is a sudden change in V_f and it starts to increase again and goes up to 1492 m/sec (100.3%).

Based on V_f inversion and the range of fluid velocities in the reservoir, we can easily identify pore fluid in the reservoir. The upper part, which is from 1 to 1.07 s, is the oil-saturated zone because the fluid velocity in this zone is 745 m/s, whereas the lower part, which is from 1.07 to 1.5 s, is the brine-saturated zone because the fluid velocity in this zone is 1492 m/s.

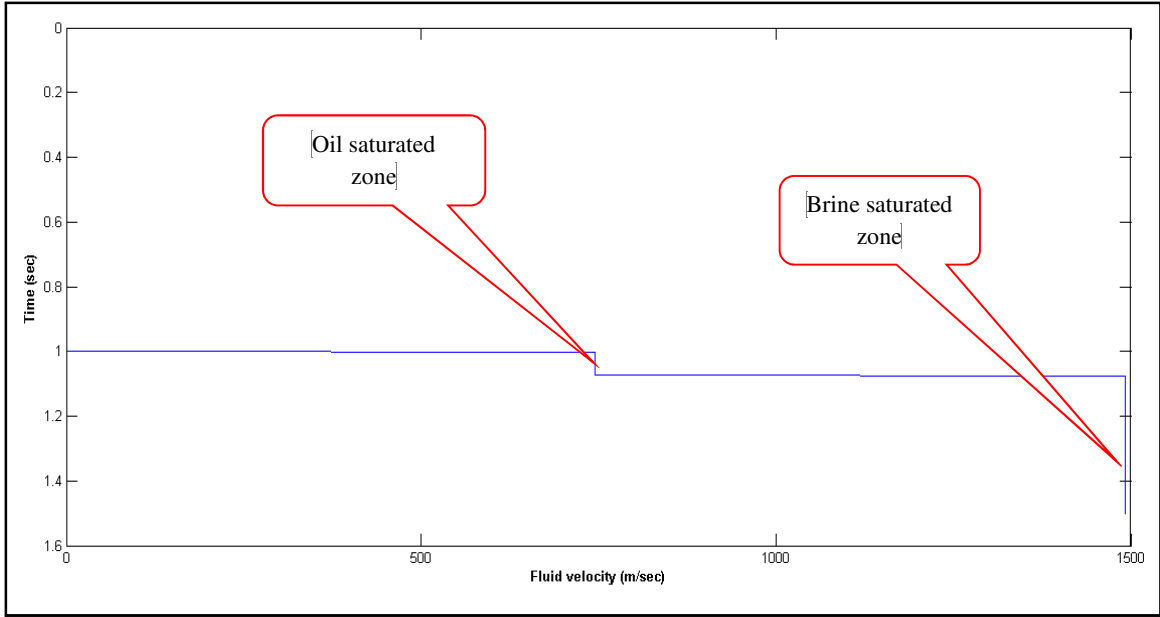


Figure 4.14: Fluid velocity plot with 20% porosity of Arab formation

4.8 30% Porosity

4.8.1 Fluid density (ρ_f)

Figure-4.15 shows the fluid density (ρ_f) plot of the trace, which is exactly in the middle of the model as well as of the reservoir. In this case, the porosity of the Arab formation is assumed to be 30% to observe the effect on fluid density. From 0 to 1 s ρ_f has no value because we do not have any fluid in the upper two layers. As we enter into the reservoir, ρ_f starts to increase from 0 to 723 Kg/m^3 . Between 1 to 1.07 s and the ρ_f remains at 723 Kg/m^3 . After 1.07 s, there is a sudden change in ρ_f and it starts to increase again and goes up to 1062 Kg/m^3 (46.9%).

Based on ρ_f inversion and the range of fluid densities in the reservoir, we can easily identify pore fluid in the reservoir. The upper part, which is from 1 to 1.07 s, is the oil saturated zone because the fluid density in this zone is 723 Kg/m^3 , whereas the lower part, which is from 1.07 to 1.5 s, is the brine saturated zone with 1062 Kg/m^3 density.

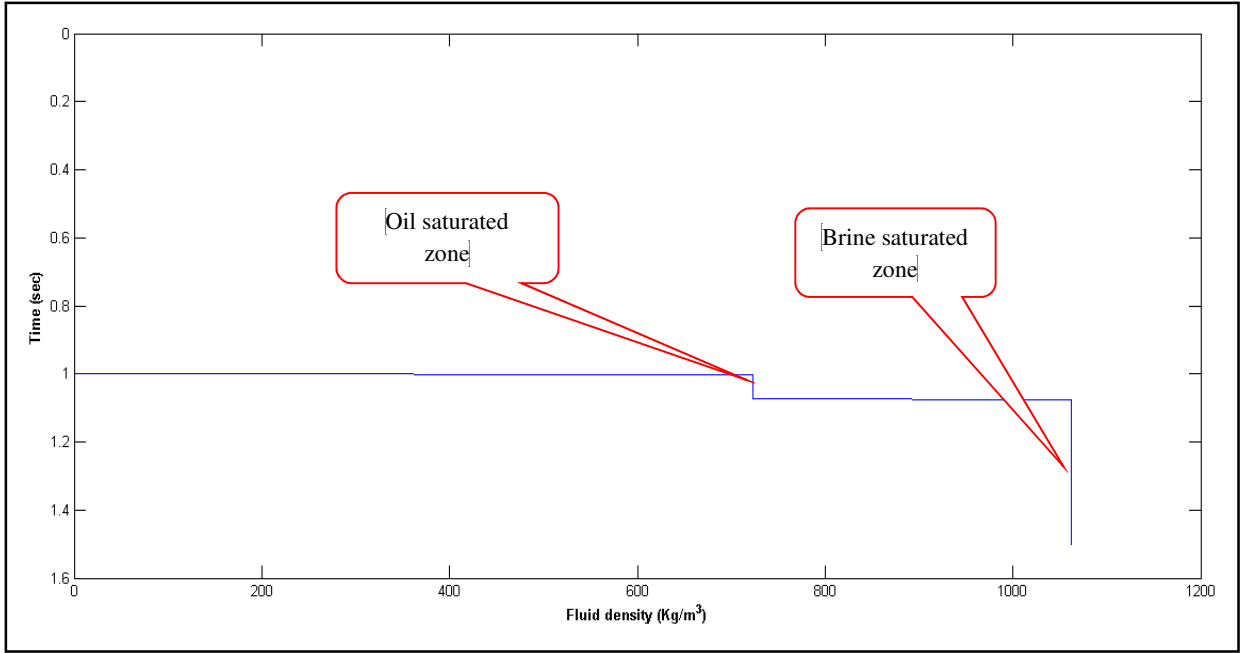


Figure 4.15: Fluid density plot with 30% porosity of Arab formation

4.8.2 Fluid velocity (V_f)

Figure-4.16 shows the fluid velocity (V_f) plot of the trace, which is exactly in the middle of the model as well as of the reservoir. In this case, the porosity of the Arab formation is assumed to be 30% to observe the effect on fluid velocity. From 0 to 1 s V_f has no value because we do not have any fluid in upper two layers. As we enter into the reservoir, V_f starts to increase from 0 to 748 m/sec, between 1 and 1.07 s the V_f remains at 748 m/sec. After 1.07 s, there is a sudden change in V_f and it starts to increase again and goes up to 1490 m/sec (99.2%).

Based on V_f inversion and the range of fluid velocities in the reservoir, we can easily identify pore fluid in the reservoir. The upper part, which is from 1 to 1.07 s, is the oil-saturated zone because the fluid velocity in this zone is 748 m/s, whereas the lower part, which is from 1.07 to 1.5 s, is the brine-saturated zone because the fluid velocity in this zone is 1490 m/s.

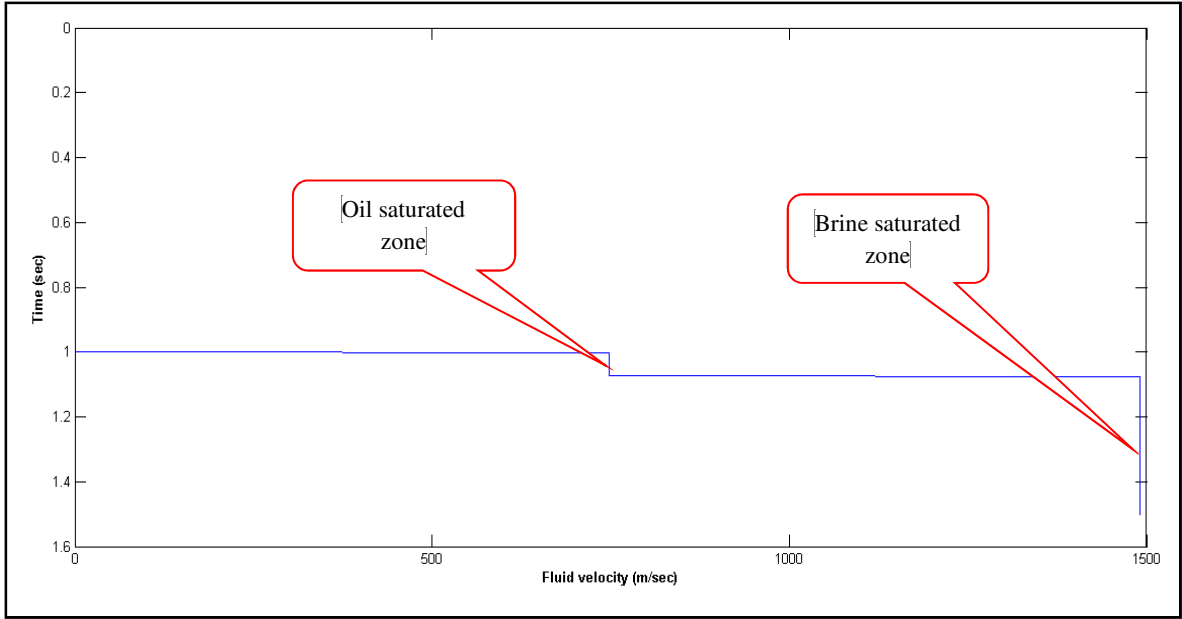


Figure 4.16: Fluid velocity plot with 30% porosity of Arab formation

CHAPTER 5

CONCLUSIONS AND RECOMMENDATIONS

5.1 Conclusions

There are various techniques and algorithms developed in the oil and gas industry to identify and characterize the pore fluid. Here, without using well log data, I tried to identify the pore fluid in my target reservoir. The final conclusions based on the results of this research are given below:

- AI, compressional bulk modulus, and saturated rock density inversion give good evidence of the presence of two different pore fluids in the reservoir due to sudden change as we move from the upper zone to the lower zone within the reservoir. Table 5.1 shows the change in the reservoir as we move from the hydrocarbon zone to the brine zone.

Table 5.1: Change in percent in AI, M and ρ_f

Cases#	Acoustic Impedance	Compressional modulus	Saturated rock density
Case-1	7.30%	5.70%	9.03%
Case-2	3.80%	4.60%	3%

- The results of fluid density and fluid velocity give better evidence and information about the pore fluids and are a helpful tool in identifying the pore fluids in the reservoir as shown in Table 5.2.

Table 5.2: Change in percent in fluid density and fluid velocity

Cases	Fluid density	Fluid velocity
Case-1	1014.74%	2900%
Case-2	46.70%	101.30%
Arab formation	46.90%	99.00%

- The percent error between the inverted fluid density and the computed fluid density for gas, live oil, and brine are almost 0% for cases 1 and 2.
- The percent error between the inverted fluid velocity and the computed fluid velocity for gas, live oil, and brine is almost 0% for cases 1 and 2
- In the case of the Arab formation, where we have different porosities, the percent error in fluid density and velocity are given in Table-5.3:

Table 5.3: Percent error analysis in the Arab formation

Fluid type	Porosity %	Computed Fluid density (Kg/m³)	Inverted Fluid density (Kg/m³)	Percent error	Computed Fluid velocity (m/sec)	Inverted Fluid velocity (m/sec)	Percent error %
Live oil	10 %	722.9	723	0.0138	745.7754	746.7897	0.136
	20 %		723	0.0138		745.7225	0.096
	30 %		723	0.0138		748.1047	0.3123
Brine	10 %	1059.624	1062	0.2238	1499	1481.383	1.175
	20 %		1062.5	0.2714		1492.46	0.436
	30 %		1062.333	0.2556		1490.372	0.5755

5.2 Recommendations

Based on the findings of the current study the following recommendations can extend the application of this study:

- This model should be integrated with AVO analysis for fluid characterization in a reservoir.
- AI inversion should be calibrated with well data to achieve better results.

References

- [1] Rosa R. L. A., Arso R. L. and Jaeghe R., Mapping Oil-Water Contact with Seismic Data in Campos Basin, Offshore Brazil, SEG Conference Paper, 1985.
- [2] Royal J. A., Logel D. J. and Lines R. L., AVO investigation of the Ben Nevis reservoir at the Hebron asset, SEG 74th Annual Meeting, 2004.
- [3] Kato A. and Stewart R., Joint AVO inversion for Time-Lapse elastic reservoir properties, SPE, 2012.
- [4] Estrada C. and Mantilla C., Tilted oil water contact in the Cretaceous Caballos Formation, Puerto Colon Field, Putumayo Basin, Colombia, SPE Asia Pacific Conference on Integrated Modeling for Asset Management held in Yokohama, 2000.
- [5] Williams M. D., The Acoustic Log Hydrocarbon Indicator, SPWLA 31st Annual Logging Symposium, 1990.
- [6] Snyder D. D. and Fleming B. D., Well logging-A 25-year perspective, Geophysics, VOL. 50, NO. 12, 1985.
- [7] Chiburis, E. F., Analysis of amplitude versus offset to detect gas/oil contacts in the Arabian Gulf, SEG, 1984.
- [8] Chiburis, E. F., Studies of amplitude versus offset to detect hydrocarbon contacts in the Arabian Arabia, SEG, 1986.

- [9] Li D. and Zhang F., Direct estimation of petrophysical properties based on AVO inversion, SEG, 2015.
- [10] Doll, H.G., Legrand, J.C. and Stratton, E.F., True Resistivity Determination from the Electric Log-Its Application to Log Analysis, API Conference Paper, 1947.
- [11] Gevers and Watson, S.W., Quantitative Interpretation of Seismic Data using Well Logs, SPE Conference Paper, 1978.
- [12] Bryant L. H., Production Well Logging Techniques, Geophysics, VOL. XXV, NO. 4, 1960.
- [13] Setyowiyoto J. and Samsuri A., oil water contact analysis and hydrocarbon saturation estimation based on well data, Regional Postgraduate conference on Engineering and Science Johore, India, 2006.
- [14] Pande N. K., Estimation of Oil Water Contact in Development Wells with the help of Variable Density Logs, SPWLA Twenty-Fourth Annual Logging Symposium, 1983.
- [15] Maver G. K. and Rasmussen B. K., Simultaneous AVO Inversion for Accurate Prediction of Rock Properties, OTC, 2004.
- [16] Chombart G. L., Well Logs in Carbonate Reservoirs, 29th Annual Meeting of the SEG, 1960.
- [17] Wyllie J. R. M., Procedures for the Direct Employment of Neutron Log data in ELECTRIC Log Interpretation, SEG Los Angeles meeting March 24, 1952.

- [18] Batzle M. and Wang Z., Seismic properties of pore fluids, *Geophysics*, VOL. 57, NO. 11, 1992.
- [19] Dutta C. N., and Ode H., Seismic reflections from a gas-water contact, *Geophysics* VOL. 48. NO. 2, 1983.
- [20] Singh R., Rao V. R. and Dco P. P., Identification of Gas-Oil Contacts by Overlay Techniques Using Wireline Log Data, *SPWLA Journal Paper*, 1998.
- [21] Hiran R. and Eugenio D., Alternative Methods of Identifying the Oil Water Contacts in Stratigraphy Columns with Multiple Reservoirs, *PWLA 55th Annual Logging Symposium*, 2014.
- [22] Ramamoorthy R. and Murphy F. W., Fluid Identification through Dynamic Modulus Decomposition in Carbonate Reservoirs, *SPWLA 39th Annual Logging Symposium*, 1998.
- [23] Steineke, Max, Bramkamp, R. A., and Sander, N. J., 1958, Stratigraphic relations of Arabian Jurassic oil in Habitat of oil: *Am. Assoc. Petroleum Geologists Symposium*, p. 1294-1329.
- [24] Power W. R. et al., *Geology of the Arabian Peninsula Sedimentary Geology of Saudi Arabia*, 1963.
- [25] Klimentos T., Attenuation of P- and S-waves as a method of distinguishing gas and condensate from oil and water, *GEOPHYSICS*, VOL. 60, NO.2, 1995.
- [26] Wilson, H. H., *Hydrocarbon habitat in main producing areas, Saudi Arabia*, 1981.
- [27] Chi X. and Han D., Reservoir properties inversion from AVO attributes, *SEG annual meeting*, 2007.

[28] Yilmaz, O., Seismic data analysis, SEG, 2001.

|

Vitae

Name	:Amjad Ali
Nationality	:Pakistani
Date of Birth	:4/15/1987
Email	:amjadjan_87@yahoo.com
Address	:V.P.O. Tano Tehsil Lahor Distt. Swabi, KPK, Pakistan
Academic Background	:M.Sc. Geophysics from Quaid-i-Azam University,Pakistan

Professional History

- Internee Spud Energy Pty. Ltd. Islamabad Pakistan, July 2015-August 2015
- Assistant Geophysicist Dewan Petroleum Pvt. Ltd. Islamabad Pakistan, May 2012-December 2014